

Galileo dust data from the jovian system: 2000 to 2003

H. Krüger^{a,b,1}, D. Bindschadler^c, S. F. Dermott^d, A. L. Graps^e, E. Grün^{b,f}, B. A. Gustafson^d, D. P. Hamilton^g, M. S. Hanner^h, M. Horányi^f, J. Kissel^a, D. Linkert^b, G. Linkert^b, I. Mannⁱ, J. A. M. McDonnell^j, R. Moissl^a, G. E. Morfill^k, C. Polanskey^c, M. Roy^c, G. Schwehm^l and R. Srama^{b,m}

- a) Max-Planck-Institut für Sonnensystemforschung, 37191 Katlenburg-Lindau, Germany
- b) Max-Planck-Institut für Kernphysik, 69029 Heidelberg, Germany
- c) Jet Propulsion Laboratory, Pasadena, California 91109, USA
- d) University of Florida, 211 SSRB, Campus, Gainesville, FL 32609, USA
- e) Department of Space Studies, Southwest Research Institute, 1050 Walnut Street, Suite 300, Boulder, Colorado, 80302, USA
- f) Laboratory for Atmospheric and Space Physics, Univ. of Colorado, Boulder, CO 80309, USA
- g) University of Maryland, College Park, MD 20742-2421, USA
- h) Astronomy Dept. 619 LGRT, University of Massachusetts, Amherst MA 01003, USA
- i) School of Science and Engineering, Kindai University, Kowakae 3-4-1, Higashi-Osaka, Osaka, 577-8502, Japan
- j) Planetary and Space Science Research Institute, The Open University, Milton Keynes, MK7 6AA, UK
- k) Max-Planck-Institut für Extraterrestrische Physik, 85748 Garching, Germany
- l) ESAC, PO Box 78, 28691 Villanueva de la Cañada, Spain
- m) Universität Stuttgart, Institut für Raumfahrtssysteme, Pfaffenwaldring 31, 70569 Stuttgart, Germany

¹Correspondence to: Harald Krüger, krueger@mps.mpg.de

Abstract

The Galileo spacecraft was the first man-made satellite of Jupiter, orbiting the planet between December 1995 and September 2003. The spacecraft was equipped with a highly sensitive dust detector that monitored the jovian dust environment between approximately 2 and 370 R_J (jovian radius $R_J = 71492$ km). The Galileo dust detector was a twin of the one flying on board the Ulysses spacecraft. This is the tenth in a series of papers dedicated to presenting Galileo and Ulysses dust data. Here we present data from the Galileo dust instrument for the period January 2000 to September 2003 until Galileo was destroyed in a planned impact with Jupiter. The previous Galileo dust data set contains data of 2883 particles detected during Galileo's interplanetary cruise and 12978 particles detected in the jovian system between 1996 and 1999. In this paper we report on the data of additional 5389 particles measured between 2000 and the end of the mission in 2003. The majority of the 21250 particles for which the full set of measured impact parameters (impact time, impact direction, charge rise times, charge amplitudes, etc.) was transmitted to Earth were tiny grains (about 10 nm in radius), most of them originating from Jupiter's innermost Galilean moon Io. They were detected throughout the jovian system and the impact rates frequently exceeded 10 min^{-1} . Surprisingly large impact rates up to 100 min^{-1} occurred in August/September 2000 when Galileo was far away ($\approx 280 R_J$) from Jupiter, implying dust ejection rates in excess of 100 kg s^{-1} . This peak in dust emission appears to coincide with strong changes in the release of neutral gas from the Io torus. Strong variability in the Io dust flux was measured on timescales of days to weeks, indicating large variations in the dust release from Io or the Io torus or both on such short timescales. Galileo has detected a large number of bigger micron-sized particles mostly in the region between the Galilean moons. A surprisingly large number of such bigger grains was measured in March 2003 within a 4-day interval when Galileo was outside Jupiter's magnetosphere at approximately $350 R_J$ jovicentric distance. Two passages of Jupiter's gossamer rings in 2002 and 2003 provided the first actual comparison of in-situ dust data from a planetary ring with the results inferred from inverting optical images. Strong electronics degradation of the dust instrument due to the harsh radiation environment of Jupiter led to increased calibration uncertainties of the dust data.

1 Introduction

The Galileo spacecraft was the first artificial satellite orbiting Jupiter. Galileo had a highly sensitive impact ionization dust detector on board which was identical with the dust detector of the Ulysses spacecraft (Grün et al., 1992a,b, 1995c). Dust data from both spacecraft were used for the analysis of e. g. the interplanetary dust complex, dust related to asteroids and comets, interstellar dust grains sweeping through the solar system, and various dust phenomena in the environment of Jupiter. References can be found in Krüger et al. (1999a,c).

In Section 1.1 we summarize results that are related to dust in the Jupiter system. A comprehensive overview of the investigation of dust in the jovian system was given by Krüger (2003) and Krüger et al. (2004).

1.1 Summary of results from the Galileo dust investigations at Jupiter

The Jupiter system was found to be a strong source of dust when in 1992 Ulysses flew by the planet and discovered streams of dust particles emanating from the giant planet's magnetosphere (Grün et al., 1993). These were later confirmed by Galileo (Grün et al., 1996a,b) and measured again by Ulysses in 2003-05 during its second flyby at the planet (Krüger et al., 2006c; Flandes and Krüger, 2007; Flandes et al., 2009). At least four dust populations were identified in the Jupiter system with Galileo (Grün et al., 1997a, 1998):

i) Streams of dust particles with high and variable impact rates throughout Jupiter's magnetosphere. They are the extension of streams discovered with Ulysses outside Jupiter's magnetosphere. The particles are about 10 nm in radius (Zook et al., 1996) and they mostly originate from the innermost Galilean moon Io (Graps et al., 2000). Because of their small sizes the charged grains strongly interact with Jupiter's magnetosphere (Horányi et al., 1997; Grün et al., 1998; Heck, 1998), and they are a natural laboratory to study dust-plasma interactions. The dust streams mostly show a dust-in-plasma behavior while only some portions of those Galileo orbits displaying the highest dust stream fluxes (Galileo orbits E4, G7, G8, C21) satisfy the minimum requirements for a dusty plasma (Graps, 2006). The dust streams served as a monitor of Io's volcanic plume activity (Krüger et al., 2003a) and as probes of the Io plasma torus (Krüger et al., 2003b). Dust charging mechanisms in Io's plumes and in the jovian magnetosphere were investigated by Graps (2001) and Flandes (2005). Dust measurements of the Cassini spacecraft at its Jupiter flyby in 2000 showed that the grains are mostly composed of sodium chloride (NaCl) formed by condensation in Io's volcanic plumes (Postberg et al., 2006).

ii) Dust clouds surrounding the Galilean moons which consist of mostly sub-micron grains (Krüger et al., 1999d, 2000, 2003c). These grains were ejected from the moons' surfaces by hypervelocity impacts of interplanetary dust particles (Krivov et al., 2003; Sremčević et al., 2003, 2005).

iii) Bigger micron-sized grains forming a tenuous dust ring between the Galilean moons. This group is composed of two sub-populations, one orbiting Jupiter on prograde orbits and

78 a second one on retrograde orbits (Colwell et al., 1998; Thiessenhusen et al., 2000). Most
79 of the prograde population is maintained by grains escaping from the clouds that surround
80 the Galilean moons (Krivov et al., 2002a,b).

81 iv) On 5 November 2002 and 21 September 2003 – before Galileo was destroyed in a
82 planned impact with Jupiter – the spacecraft traversed Jupiter’s gossamer ring twice and
83 provided the first in-situ measurements of a dusty planetary ring (Krüger, 2003; Moissl,
84 2005; Hamilton and Krüger, 2008; Krüger et al., 2009) which is also accessible with astro-
85 nomical imaging techniques. These fly-throughs revealed previously unknown structures
86 in the gossamer rings: a drop in the dust density between the moons Amalthea and Thebe,
87 grains orbiting Jupiter on highly inclined orbits and an increase in the number of small
88 grains in the inner regions of the rings as compared to the regions further away from the
89 planet. All these features can nicely be explained by electromagnetic forces on the grains
90 that shape the gossamer rings (Hamilton and Krüger, 2008).

91 **1.2 The Galileo and Ulysses dust data papers**

92 This is the tenth paper in a series dedicated to presenting both raw and reduced data from
93 the Galileo and Ulysses dust instruments. Grün et al. (1995c, hereafter Paper I) described
94 the reduction process of Galileo and Ulysses dust data. In the even-numbered Papers II,
95 IV, VI and VIII (Grün et al., 1995a; Krüger et al., 1999a, 2001a, 2006b) we presented the
96 Galileo data set spanning the ten year time period from October 1989 to December 1999.
97 The present paper extends the Galileo data set from January 2000 to September 2003,
98 which covers the Galileo Millenium mission and two traverses of Jupiter’s gossamer ring
99 until the spacecraft impacted Jupiter on 21 September 2003. Companion odd-numbered
100 Papers III, V, VII, IX and XI (Grün et al., 1995b; Krüger et al., 1999c, 2001b, 2006a,
101 2010) provide the entire dust data set measured with Ulysses between 1990 and 2007. An
102 overview of our Galileo dust data papers and mission highlights is given in Table 1.

103 **Insert Table 1**

104 The main data products are a table of the number of all impacts determined from the par-
105 ticle accumulators and a table of both raw and reduced data of all “big” impacts received
106 on the ground. The information presented in these papers is similar to data which we are
107 submitting to the various data archiving centres (Planetary Data System, NSSDC, etc.).
108 The only difference is that the paper version does not contain the full data set of the large
109 number of “small” particles, and the numbers of impacts deduced from the accumulators
110 are typically averaged over several days. Electronic access to the complete data set includ-
111 ing the numbers of impacts deduced from the accumulators in full time resolution is also
112 possible via the world wide web: <http://www.mpi-hd.mpg.de/dustgroup/>.

113 This paper is organised similarly to our previous papers. Section 2 gives a brief overview
114 of the Galileo mission with particular emphasis on the time period 2000-2003, the dust
115 instrument operation and lists important mission events in the time interval 2000-2003

116 considered in this paper. A description of the new Galileo dust data set for 2000-2003
117 together with a discussion of the detected noise and dust impact rates is given in Section 3.
118 Section 4 analyses and discusses various characteristics of the new data set. Finally, in
119 Section 5 we discuss results on jovian dust achieved with this new data set, and in Section 6
120 we summarise our results.

121 **2 Mission and instrument operations**

122 **2.1 Galileo mission**

123 Galileo was launched on 18 October 1989. Two flybys at Earth and one at Venus between
124 1990 and 1992 gave the spacecraft enough energy to leave the inner solar system. During
125 its interplanetary voyage Galileo had close encounters with the asteroids Gaspra and Ida.
126 On 7 December 1995 the spacecraft arrived at Jupiter and was injected into a highly elliptical
127 orbit about the planet, becoming the first spacecraft orbiting a planet of the outer solar
128 system. Galileo performed 34 revolutions about Jupiter until 21 September 2003 when the
129 spacecraft was destroyed in a planned impact with Jupiter.

130 Galileo’s trajectory during its orbital tour about Jupiter from January 2000 to September
131 2003 is shown in Figure 1. Galileo had regular close flybys at Jupiter’s Galilean
132 moons. Eight such encounters occurred in the 2000-2003 interval (1 at Europa, 4 at Io,
133 2 at Ganymede, 1 at Callisto) plus one at Amalthea (Table 2). Galileo orbits are labelled
134 with the first letter of the Galilean moon which was the encounter target during that orbit,
135 followed by the orbit number. For example, “G29” refers to a Ganymede flyby in orbit 29.
136 Satellite flybys always occurred within two days of Jupiter closest approach (pericentre
137 passage). Detailed descriptions of the Galileo mission and the spacecraft were given by
138 Johnson et al. (1992) and D’Amario et al. (1992).

139

Insert Table 2

140

Insert Figure 1

141 Galileo was a dual spinning spacecraft with an antenna that pointed antiparallel to the posi-
142 tive spin axis. During most of the initial 3 years of the mission the antenna pointed towards
143 the Sun (Paper II). Since 1993 the antenna was usually pointed towards Earth. Deviations
144 from the Earth pointing direction in 2000-2003, the time period considered in this paper,
145 are shown in Figure 2. Sharp spikes in the pointing deviation occurred when the spacecraft
146 was turned away from the nominal Earth direction for dedicated imaging observations with
147 Galileo’s cameras or for orbit trim maneuvers with the spacecraft thrusters. These spikes
148 lasted typically several hours. From January to September 2003, the Galileo pointing de-
149 viated significantly from the Earth pointing direction for a long time interval. Table 2
150 lists significant mission and dust instrument events for 2000-2003. Comprehensive lists of
151 earlier events can be found in Papers II, IV, VI and VIII.

152

Insert Figure 2

153 **2.2 Dust detection geometry**

154 The Dust Detector System (DDS) was mounted on the spinning section of Galileo and the
155 sensor axis was offset by 60° from the positive spin axis (an angle of 55° was erroneously
156 stated in publications before). A schematic view of the Galileo spacecraft and the geometry
157 of dust detection is shown in the inset in Figure 1.

158 The rotation angle measured the viewing direction of the dust sensor at the time of a dust
159 impact. During one spin revolution of the spacecraft the rotation angle scanned through a
160 complete circle of 360° . At rotation angles of 90° and 270° the sensor axis lay nearly in
161 the ecliptic plane, and at 0° it was close to the ecliptic north direction. DDS rotation angles
162 are taken positive around the negative spin axis of the spacecraft which pointed towards
163 Earth. This is done to facilitate comparison of the Galileo spin angle data with those taken
164 by Ulysses, which, unlike Galileo, had its positive spin axis pointed towards Earth (Grün
165 et al., 1995c).

166 The nominal field-of-view (FOV) of the DDS sensor target was 140° . A smaller FOV
167 applies to a subset of jovian dust stream particle impacts – the so-called class 3 impacts
168 in amplitude range AR1 (Krüger et al., 1999b, *cf.* Paper I and Section 3 for a definition
169 of these parameters) while the nominal target size should be applied to class 2 jovian dust
170 stream impacts. For all impacts which are not due to jovian dust stream particles a larger
171 FOV of 180° should be applied because the inner sensor side wall turned out to be almost
172 as sensitive to larger dust impacts as the target itself (Altobelli et al., 2004; Willis et al.,
173 2004, 2005). These different sensor fields-of-view and the corresponding target sizes are
174 summarised in Table 3.

175

Insert Table 3

176 During one spin revolution of the spacecraft the sensor axis scanned a cone with 120°
177 opening angle towards the anti-Earth direction. Dust particles that arrived from within
178 10° of the positive spin axis (anti-Earth direction) could be detected at all rotation angles,
179 whereas those that arrived at angles from 10° to 130° from the positive spin axis could be
180 detected over only a limited range of rotation angles. Note that these angles refer to the
181 nominal sensor field-of-view of 140° .

182 **2.3 Data transmission**

183 In June 1990 the dust instrument was reprogrammed for the first time after launch and
184 since then the instrument memory could store 46 instrument data frames (with each frame
185 comprising the complete data set of an impact or noise event, consisting of 128 bits, plus
186 ancillary and engineering data; *cf.* Papers I and II). The dust instrument time-tagged each

187 impact event with an 8 bit word allowing for the identification of 256 unique steps. In
188 1990 the step size of this time word was set to 4.3 hours. Hence, the total accumulation
189 time after which the time word was reset and the time labels of older impact events became
190 ambiguous was $256 \times 4.3 \text{ h} \simeq 46 \text{ days}$.

191 During a large fraction of Galileo's orbital mission about Jupiter dust detector data were
192 transmitted to Earth in the so-called realtime science mode (RTS). In RTS mode, dust
193 data were read out either every 7.1 or every 21.2 minutes – depending on the spacecraft
194 data transmission rate – and directly transmitted to Earth with a rate of 3.4 or 1.1 bits per
195 second, respectively. Additionally, Galileo had the so-called record mode. In this mode
196 data were read out from the dust instrument memory with 24 bits per second, recorded on
197 Galileo's tape recorder and transmitted to Earth up to several weeks later. Recorded data
198 were received during three satellite flybys in 2000 during short periods of $\sim \pm 1/2$ hour
199 around closest approach to the satellite, and for ~ 3.8 hours during Galileo's gossamer ring
200 passage on 5 November 2002 (Table 2). Details of the various data transmission modes of
201 Galileo are also given in Table 4.

202 **Insert Table 4**

203 In RTS and record mode the time between two readouts of the instrument memory deter-
204 mined the number of events in a given time period for which their complete information
205 could be transmitted. Thus, the complete information on each impact was transmitted to
206 Earth when the impact rate was below one impact per either 7.1 or 21.2 minutes in RTS
207 mode or one impact per minute in record mode, respectively (Table 4). If the impact rate
208 exceeded these values, the detailed information of older events was lost because the full
209 data set of only the latest event was stored in the dust instrument memory.

210 Furthermore, in RTS and record mode the time between two readouts also defined the
211 accuracy with which the impact time is known. Hence, the uncertainty in the impact time
212 is 7.1 or 21.2 minutes in RTS mode and about one minute in record mode, respectively.

213 In RTS and record mode only seven instrument data frames were read out at a time and
214 transmitted to Earth rather than the complete instrument memory. Six of the frames con-
215 tained the information of the six most recent events in each amplitude range. The seventh
216 frame belonged to an older event read out from the instrument memory (FN=7) and was
217 transmitted in addition to the six new events. The position in the instrument memory from
218 which this seventh frame was read changed for each readout so that after 40 readouts the
219 complete instrument memory was transmitted (note that the contents of the memory may
220 have changed significantly during the time period of 40 readouts if high event rates oc-
221 curred).

222 RTS data were usually obtained when Galileo was in the inner jovian system where rela-
223 tively high dust impact rates occurred. During time intervals when Galileo was in the outer
224 jovian magnetosphere dust data were usually received as instrument memory-readouts
225 (MROs). MROs returned event data which had accumulated in the instrument memory
226 over time. The contents of all 46 instrument data frames of the dust instrument was read

227 out during an MRO and transmitted to Earth. If too many events occurred between two
228 MROs, the data sets of the oldest events became overwritten in the memory and were lost.
229 Although the entire memory was read out during an MRO, the number of data sets of
230 new events that could be transmitted to Earth in a given time period was much smaller than
231 with RTS data because MROs occurred much less frequently (Table 4). During times when
232 only MROs occurred, the accuracy of the impact time was defined by the increment of the
233 instrument's internal clock, i.e. 4.3 hours.

234 In 2000-2003, RTS and record data were obtained during a period of 570 days (Figure 1)
235 which amounts to about 40% of the total almost 4-year period. During the remaining
236 times when the dust instrument was operated in neither RTS nor record mode, a total of 59
237 MROs occurred at approximately 2 to 3 week intervals. Until the end of 2002, MROs were
238 frequent enough so that usually no ambiguities in the time-tagging occurred (i.e. MROs
239 occurred at intervals smaller than 46 days).

240 The last MRO for the entire Galileo mission occurred at the end of 2002 on day 02-363.
241 In 2003 we received dust data neither as MROs nor as record data. Only RTS data were
242 received during rather short time intervals: about one week from 03-063 to 03-070 and
243 a total of about two days between 03-255 and 03-264 before the spacecraft hit Jupiter
244 (Table 2). No dust data were obtained outside these intervals in 2003.

245 Several resets of the dust instrument's internal clock occurred during the long periods with-
246 out data transmission in 2003, leading to ambiguities in the impact time of some dust
247 impacts. One clock reset occurred during the first data gap between 02-363 and 03-063
248 and four resets in the second gap between 03-070 and 03-255. Furthermore, due to data
249 transmission problems, the time tagging was lost for the events transmitted in the interval
250 03-063 to 03-070. Consequently, the impact time of two events which occurred between
251 02-363 and 03-063 is completely unknown. We have therefore set their impact time to
252 03-030 (these grains are indicated by horizontal bars in Figure 9). For seven data sets
253 transmitted between 03-063 and 03-070 the impact time could be determined with an ac-
254 curacy of approximately one day from the time tagging of test pulses that were routinely
255 performed by the dust instrument (see also Section 5.4).

256 **2.4 Dust instrument operation**

257 During Galileo's earlier orbital mission about Jupiter strong channeltron noise was usu-
258 ally recorded while Galileo was within about $20R_J$ distance from Jupiter (Jupiter radius,
259 $R_J = 71,492\text{ km}$). The details are described in Papers VI and VIII and not repeated here.
260 Furthermore, due to degradation of the channeltron, the high voltage setting (HV) had to
261 be raised two times in 1999 (Paper VIII). At the beginning of the year 2000, i.e. at the
262 beginning of the time period considered in this paper, the dust instrument was operated
263 in the following nominal configuration: the channeltron high voltage was set to 1250 V
264 ($HV = 4$), the event definition status was set such that only the ion-collector channel could
265 initiate a measurement cycle ($EVD = I$) and the detection thresholds for the charges on the
266 ion-collector, channeltron, electron-channel and entrance grid were set ($SSEN = 0, 1, 1, 1$).

267 This configuration effectively prevented dead time of the instrument due to channeltron
268 noise (serious channeltron noise rates with $CN > 10$ occurred only during seven short
269 time intervals in orbit A34 on day 02-309 when Galileo was inside Io's orbit and lasted
270 only between several seconds and less than a minute. The resulting dead time is negligible
271 because of its random occurrence and short duration). Due to degradation of the channel-
272 tron (Section 2.5) the channeltron high voltage was raised two additional times on days
273 00-309 and 01-352 in order to maintain a rather constant instrument sensitivity for dust
274 impacts (Table 2).

275 During the Jupiter orbital tour of Galileo, orbit trim maneuvers (OTMs) were executed
276 around perijove and apojove passages to target the spacecraft to close encounters with the
277 Galilean moons. Many of these maneuvers required changes in the spacecraft attitude off
278 the nominal Earth pointing direction (Figure 2). Additionally, dedicated spacecraft turns
279 occurred typically in the inner jovian system within a few days around perijove passage to
280 allow for imaging observations with Galileo's cameras or to maintain the nominal Earth
281 pointing direction.

282 In the time interval considered in this paper a total of five spacecraft anomalies (safings)
283 occurred on days 00-055, 02-017, 02-047, 02-274, and 02-309 (Table 2). Three of these
284 anomalies occurred in the inner jovian system in the region where the highest radiation
285 levels were collected by the spacecraft, and recovery usually took several days. Although
286 the dust instrument continued to measure dust impacts, the collected data could not be
287 transmitted to Earth during the recovery and most of them were lost.

288 No reprogramming of the instrument's onboard computer was necessary in the 2000-2003
289 time interval. In fact, the last reprogramming for the entire Galileo mission took place on
290 4 December 1996 when two overflow counters were added for the so-called AR1 impacts
291 in classes 2 and 3 (Paper VI). With these overflow counters, all accumulator overflows
292 could be recognized in these two channels in the 2000-2003 interval. It is very unlikely
293 that unrecognized overflows occurred in the higher amplitude ranges. The only exception
294 is day 02-309 when Galileo was in the gossamer ring region and the instrument continued
295 to collect data after the spacecraft anomaly (see also Section 5.5). Here unrecognized over-
296 flows have likely occurred in amplitude range AR1, class 1 (channel AC11) and amplitude
297 range AR2 (except channel AC32), while the higher amplitude ranges AR3 and AR4 were
298 most likely free of overflows. See Section 3.1 for a description of the amplitude ranges and
299 quality classes of dust impacts.

300 **2.5 Dust instrument electronics degradation**

301 Analysis of the impact charges and rise times measured by the dust instrument revealed
302 strong degradation of the instrument electronics which was most likely caused by the
303 harsh radiation environment in the inner jovian magnetosphere. A detailed analysis was
304 published by Krüger et al. (2005). Here we recall the most significant results: a) the sensi-
305 tivity of the instrument for dust impacts and noise had dropped. b) the amplification of the
306 charge amplifiers had degraded, leading to reduced impact charge values Q_I and Q_E . c)

307 drifts in the target and ion collector rise time signals lead to prolonged rise times t_I and t_E .
308 d) degradation of the channeltron required increases in the channeltron high voltage (Ta-
309 ble 2). In particular, a) requires a time-dependent correction when comparing dust fluxes
310 early in the Galileo Jupiter mission with later measurements; b) and c) affect the mass and
311 speed calibration of the dust instrument. After 2000, masses and speeds derived from the
312 instrument calibration have to be taken with caution because the electronics degradation
313 was very severe. Only in cases where impact speeds are known from other arguments can
314 corrected masses of particles be derived (e.g. the dust cloud measurements in the vicinity
315 of the Galilean moons or Galileo's gossamer ring passages). On the other hand, given the
316 uncertainty in the impact calibration of a factor of two in the speed and that of a factor of
317 ten in the mass, the increased uncertainty due to the electronics degradation was compar-
318 atively small before 2000 (it should be noted that the dust data until end 1999 published
319 earlier – Papers II, IV, VI and VIII – remain unchanged). In particular, no corrections for
320 dust fluxes, grain speeds and masses are necessary until end 1999 and results obtained with
321 this data set in earlier publications remain valid. Beginning in 2000, however, the degrada-
322 tion became so severe that the calibrated speeds and masses have to be considered as lower
323 and upper limits, respectively (see also Section 3.3).

324 **3 Impact events**

325 **3.1 Event classification and noise**

326 The dust instrument classified all events – real dust impacts and noise events – into one of
327 24 different categories (6 amplitude ranges for the charge measured on the ion collector grid
328 and 4 event classes) and counted them in 24 corresponding 8 bit accumulators (Paper I).
329 In interplanetary space most of the 24 categories were relatively free from noise and only
330 sensitive to real dust impacts. The details of the noise behaviour in interplanetary space
331 can be found in Papers II and IV.

332 In the extreme radiation environment of the jovian system, a different noise response of
333 the instrument was recognized: especially within about $20 R_J$ from Jupiter class 1 and
334 class 2 were contaminated with noise while class 3 was almost always noise-free (Krüger
335 et al., 1999b). Analysis of the dust data set from Galileo's entire Jupiter mission showed
336 that noise events could reliably be eliminated from class 2 (Krüger et al., 2005) while
337 most class 1 events detected in the jovian environment showed signatures of being noise
338 events. For most of Galileo's Jupiter mission we therefore consider the class 3 and the
339 noise-removed class 2 impacts as the complete set of dust data. Apart from a missing third
340 charge signal – class 3 has three charge signals and class 2 only two – there is no physical
341 difference between dust impacts categorized into class 2 or class 3. In particular, we usually
342 classify all class 1 and class 0 events detected in the jovian environment as noise.

343 The only exceptions are the passages through Jupiter's gossamer rings in 2002 and 2003
344 where a somewhat different noise response of the instrument was recognized (Moissl,

345 2005). Here, good dust impacts could also be identified in class 1. In Table 5 we show
346 the noise identification scheme applied to the data from the gossamer ring passages ob-
347 tained while Galileo was within Io’s orbit.

348 **Insert Table 5**

349 To summarise, noise was removed from the data set we present here with two different
350 criteria: data obtained outside Io’s orbit were processed according to the criteria derived
351 by Krüger et al. (2005), while data obtained inside Io’s orbit were noise-removed with the
352 criteria of Moissl (2005) (Table 5). Degradation of the instrument electronics was taken
353 into account beginning in 1997 (Paper VIII). The derivation of the noise contamination
354 factor f_{noi} for class 2 was described in Paper VI and is not repeated here.

355 In this paper the terms ”small“ and ”big“ have the same meaning as in Papers IV, VI
356 and VIII (which is different from the terminology of Paper II). Here, we call all particles
357 in the amplitude ranges 2 and higher (AR2-6) ”big“. Particles in the lowest amplitude
358 range (AR1) are called ”small“. This distinction separates the small jovian dust stream
359 particles from bigger grains which are mostly detected between the Galilean moons (see
360 also Section 3.2).

361 Table 6 lists the number of all dust impacts and noise events identified with the dust in-
362 strument in the 2000-2003 interval as deduced from the accumulators of classes 2 and 3.
363 Depending on the event rate the numbers are given in intervals from half a day to a few
364 weeks (the numbers with the highest time resolution are available in electronic form only
365 and are provided to the data archiving centres). For impacts in these two classes in the
366 lowest amplitude range AR1 the complete data sets for only 2% of all detected events were
367 transmitted, the remaining 98% of events were only counted. About 32% of all data sets
368 for events in the higher amplitude ranges were transmitted. We give only the number of
369 events in classes 2 and 3 because they have been shown to contain real dust impacts dur-
370 ing the entire Jupiter mission: class 3 is almost always noise free (although Krüger et al.
371 (1999b) found indications for a very small number of noise events in class 3, AR1, in the
372 inner jovian system). Class 2 is strongly contaminated by noise events in the inner jovian
373 system (within about $15 R_J$ from Jupiter).

374 **Insert Table 6**

375 In the 2000-2003 interval Galileo had a total of eight targeted flybys at the Galilean moons
376 plus one at Amalthea (Table 2). During the flybys at the Galilean moons no ejecta particles
377 from the moons could be detected because of unfavourable detection geometry. During
378 the Amalthea flyby in A34, however, the dust instrument had the right detection geometry.
379 Taking the recently determined mass of Amalthea (Anderson et al., 2005), its Hill radius is
380 $r_{\text{Hill}} \sim 130$ km, only slightly larger than the moon itself. Galileo’s closest approach distance
381 was 244 km from the moon’s centre so that the spacecraft did not cross the Hill sphere
382 where an increased dust density was expected. In fact, no increase in the dust impact rate
383 could be identified, consistent with our expectations (Krüger et al., 2009).

384 **3.2 Dust impact rates**

385 Figure 3 shows the dust impact rate recorded by the dust instrument in 2000-2003 as de-
386 duced from the class 2 and 3 accumulators. The impact rate measured in the lowest ampli-
387 tude range (AR1) and the one measured in the higher amplitude ranges (AR2-6) are shown
388 separately because they reflect two distinct populations of dust. Until early 2002 AR1 con-
389 tains mostly stream particles which were measured throughout the jovian system. Bigger
390 particles (AR2-6) were mostly detected in the region between the Galilean moons.

391 Between the perijove passages I33 and A34 in 2002 a low background rate of a few times
392 10^{-4} min^{-1} was measured in AR1 which is at least an order of magnitude higher than
393 dust impact rates measured with Galileo and Ulysses in interplanetary space (Grün et al.,
394 1997b). These impacts show a broad distribution over all rotation angles (Figure 9) while
395 stream particles were expected to approach from rotation angles around 90° most of the
396 time in 2002, similar to the earlier Galileo orbits in 2000 and 2001. These grains could
397 be stream particles approaching from a much broader range of directions as was reported
398 from the dust measurements with Cassini during Jupiter flyby (Sascha Kempf, personal
399 communication).

400 During the gossamer ring passages impacts were measured in all amplitude ranges AR1-4
401 (Section 5.5). Note that the impact rate in AR1 was usually at least one to two orders of
402 magnitude higher than that for the big particles. Diagrams showing the AR1 impact rate
403 with a much higher time resolution in the inner jovian system are given in Figure 4, and
404 Galileo's gossamer ring passages are discussed in detail by Krüger et al. (2009).

405

Insert Figure 3

406

Insert Figure 4

407 In the inner jovian system the impact rates of AR1 particles frequently exceeded 10 min^{-1} .
408 An exceptionally large dust impact rate was recorded during the orbit G28 in the outer
409 jovian system when Galileo was approximately $280 R_J$ away from Jupiter (Section 5.2 and
410 Figure 12). This represents one of the highest dust ejection rates of Io recorded during the
411 entire Galileo Jupiter mission and is likely connected with a single strong volcanic eruption
412 on Io (Krüger et al., 2003a; Geissler et al., 2004).

413 **3.3 Event tables**

414 Table 7 lists the data sets for all 224 big particles detected between 1 January 2000 and 21
415 September 2003 for which the complete information exists. Class 1 and class 2 particles
416 were separated from noise by applying the criteria developed by Krüger et al. (1999b,
417 2005) and Moissl (2005) (Section 3.1). We do not list the small stream particles (AR1)
418 in Table 7 because their masses and velocities are outside the calibrated range of the dust

419 instrument and they are by far too numerous to be listed here. The complete information of
420 a total of 5165 small (AR1) dust particles was transmitted in 2000-2003. These are mostly
421 stream particles which are believed to be about 10 nm in size and their velocities exceed
422 200 km s^{-1} (Zook et al., 1996). Any masses and velocities derived for these particles with
423 existing calibration algorithms would be unreliable. The full data set for all 5389 particles
424 is submitted to the data archiving centres and is available in electronic form. A total number
425 of 7566 events (dust plus noise in all amplitude ranges and classes) were transmitted in
426 2000-2003, each with a complete data set.

427 **Insert Table 7**

428 In Table 7 dust particles are identified by their sequence number and their impact time.
429 Gaps in the sequence number are due to the omission of the small particles. The time error
430 value (TEV) which was introduced for the data set from the Jupiter mission because of the
431 large differences in the timing accuracy of the dust instrument in the various data readout
432 modes is listed next (see Table 4 and Paper VI for details). Then the event category –
433 class (CLN) and amplitude range (AR) – are given. Raw data as transmitted to Earth are
434 displayed in the next columns: sector value (SEC) which is the spacecraft spin orientation
435 at the time of impact, impact charge numbers (IA, EA, CA) and rise times (IT, ET), time
436 difference and coincidence of electron and ion signals (EIT, EIC), coincidence of ion and
437 channeltron signal (IIC), charge reading at the entrance grid (PA) and time (PET) between
438 this signal and the impact. Then the instrument configuration is given: event definition
439 (EVD), charge sensing thresholds (ICP, ECP, CCP, PCP) and channeltron high voltage step
440 (HV). See Paper I for further explanation of the instrument parameters, except TEV which
441 was introduced in Paper VI.

442 The next four columns in Table 7 give information about Galileo’s orbit: ecliptic longitude
443 and latitude (LON, LAT) and distance from Jupiter (D_{Jup} , in R_J). The next column gives
444 the rotation angle (ROT) as described in Section 2. Whenever this value is unknown, ROT
445 is arbitrarily set to 999. This occurs 71 times in the full data set that includes the small
446 particles. Then follows the pointing direction of the instrument at the time of particle
447 impact in ecliptic longitude and latitude (S_{LON} , S_{LAT}). When ROT is not valid, S_{LON} and
448 S_{LAT} are also useless and set to 999. Mean impact velocity (v) and velocity error factor
449 (VEF, i.e. multiply or divide stated velocity by VEF to obtain upper or lower limits) as
450 well as mean particle mass (m) and mass error factor (MEF) are given in the last columns.
451 For $\text{VEF} > 6$, both velocity and mass estimates are invalid and should be discarded.

452 Beginning in 2000 the degradation of the dust instrument electronics became very severe,
453 leading to artificially too long rise times and reduced charge amplitudes. The calibrated
454 mass and speed values for $\text{VEF} < 6$ listed in Table 7 should thus be considered as lower
455 limits for the impact velocity and upper limits for the particle mass throughout the 2000-
456 2003 interval.

457 No intrinsic dust charge values are given (Svestka et al., 1996). Even though the charge
458 carried by the dust grains is expected to be larger in the jovian magnetosphere than in

459 interplanetary space the charge measured on the entrance grid of the dust instrument did
460 not give any convincing results yet. Reliable charge measurements for interplanetary dust
461 grains and for dust in Saturn’s E ring were recently reported for the Cassini dust detector
462 (Kempf et al., 2004, 2006). These measurements may lead to an improved understanding
463 of the charge measurements of Ulysses and Galileo in the future.

464 Entries for the parameter PA in Table 7 sometimes have values between 49 and 63 although
465 the highest possible value allowed by the instrument electronics is 48 (Paper I). This is also
466 inherent in all Galileo and Ulysses data sets published earlier (Papers II to IX) and it is due
467 to a bit flip. According to our present understanding the correct PA values are obtained by
468 subtracting 32 from all entries which have values between 49 and 63. Values of 48 and
469 lower should remain unchanged.

470 4 Analysis

471 The positive charge measured on the ion collector, Q_I , is the most important impact param-
472 eter determined by the dust instrument because it is rather insensitive to noise. Figure 5
473 shows the distribution of Q_I for the full 2000-2003 data set (small and big particles to-
474 gether). Ion impact charges were only detected over four orders of magnitude instead
475 of the entire range of six orders of magnitude the instrument could measure. Note that
476 the saturation limit of the instrument was at about $\sim 10^{-8}$ C but the maximum measured
477 charge was $Q_I = 9.7 \times 10^{-11}$ C, well below the saturation limit. This is most likely due to
478 instrument degradation (Section 2.5 and Krüger et al., 2005).

479 The impact charge distribution of the big particles ($Q_I > 10^{-13}$ C) follows a power law
480 with index -0.15 and is shown as a dashed line in Figure 5 (if we exclude the particles
481 from the region inside Io’s orbit the slope is reduced somewhat to -0.04). This slope is
482 flatter than the values of approximately $-1/3$ derived for the jovian system from the 1996-
483 1999 Galileo data set (Papers VI and VIII). Whether this flattening is due to changes in the
484 particle properties or due to electronics degradation remains unclear. Note that the jovian
485 stream particles (AR1) were excluded from the power law fit.

486

Insert Figure 5

487 In Figure 5 the small stream particles ($Q_I < 10^{-13}$ C) are squeezed into the two leftmost
488 histogram bins. In order to investigate their behaviour in more detail we show their num-
489 ber per individual digital step separately in Figure 6. The distribution flattens for impact
490 charges below 2×10^{-14} C. Such a flattening was also evident in the earlier data sets (Pa-
491 pers II, IV, VI and VIII), indicating the sensitivity threshold of the dust instrument may
492 not be sharp. The impact charge distribution for small particles with $Q_I > 2 \times 10^{-14}$ C
493 follows a power law with index -4.7 . It is very close to the slope found from the 1996
494 Galileo data set (-4.5 , Paper VI) and somewhat steeper than the value measured in 1997-
495 1999 (-3.6 , Paper VIII). The charge distribution strongly increases towards smaller impact

496 charges. Note that the distribution of the stream particles is much steeper than that of the
497 big particles shown in Figure 5. Interestingly, if we restrict the time interval to the period
498 between 00-220 and 00-250 when Galileo was outside the jovian magnetosphere in orbit
499 G28 the stream particles show a somewhat steeper slope of -5.9 (not shown here).

500 **Insert Figure 6**

501 The ratio of the channeltron charge Q_C and the ion collector charge Q_I is a measure of the
502 channeltron amplification A which is an important parameter for dust impact identification
503 (Paper I). The in-flight channeltron amplification was monitored in Papers II, IV, VI and
504 VIII for the initial ten years of the Galileo mission to identify possible degrading of the
505 channeltron. In the earlier mission the amplification $A = Q_C/Q_I$ for a channeltron high
506 voltage setting of 1020 V ($HV = 2$) determined from impacts with $10^{-12} \text{ C} \leq Q_I \leq 10^{-10} \text{ C}$
507 was in the range $1.4 \lesssim A \lesssim 1.8$. No significant channeltron degradation was evident until
508 the end of 1996. In the 1997-1999 interval (Paper VIII) a value of $A \simeq 0.7$ was found which
509 indicated serious channeltron degradation. As a consequence, the channeltron high voltage
510 was raised two times (on days 99-305 and 99-345) to return to the original amplification
511 factor.

512 Here we repeat the same analysis for the 2000-2003 interval. Figure 7 shows the charge
513 ratio Q_C/Q_I as a function of Q_I for a constant high voltage, HV, as in the previous papers.
514 Here we show data for $HV = 6$. The charge ratio Q_C/Q_I determined for $10^{-12} \text{ C} \leq Q_I \leq$
515 10^{-10} C is $A \simeq 1.6$ and is obtained from 65 impacts. The data for $HV = 4$ and $HV = 5$
516 (time intervals 00-001 to 00-209 and 00-209 to 01-352) give $A \simeq 1.3$ and $A \simeq 0.5$, respec-
517 tively. These values, however, are derived from only 9 and 15 impacts, respectively, and
518 therefore have a much lower statistical significance. The amplification for $HV = 6$ is close
519 to the value from the interplanetary cruise and the early Jupiter mission, showing that the
520 original channeltron amplification could be roughly reestablished. Details of the dust in-
521 strument degradation due to the harsh radiation environment in the jovian magnetosphere
522 are described by Krüger et al. (2005, see also Section 2.5). It should be noted that the ratio
523 Q_C/Q_I is entirely determined by the instrument performance. It does not depend upon the
524 properties of the detected particles.

525 **Insert Figure 7**

526 Figure 8 displays the calibrated masses and velocities of all 5389 dust grains detected in
527 the 2000-2003 interval. Although the range of impact velocities calibrated in the labora-
528 tory extended from 2 to 70 km s^{-1} , the measured impact speeds ranged only up to about
529 20 km s^{-1} . This is caused by the degradation of the dust instrument electronics which lead
530 to extended rise time measurements and, hence, impact velocities which are artificially
531 too low, and calibrated grain masses artificially too large. This becomes apparent when
532 comparing Figure 8 with the corresponding figures in the earlier Papers II, IV, VI and VIII
533 where the measured range of impact speeds extends up to 70 km s^{-1} . *Therefore, due to the*

534 *strong electronics degradation, all calibrated impact speeds and masses in the time inter-*
535 *val considered in this paper should be considered as lower and upper limits, respectively.*
536 Any clustering of the velocity values is due to discrete steps in the rise time measurement
537 but this quantization is much smaller than the velocity uncertainty. For further details of the
538 mass and velocity calibration the reader is referred to the description of the mass-velocity
539 diagrams in our earlier papers.

540

Insert Figure 8

541 The impact direction of the dust particles detected in the 2000-2003 interval is shown in
542 Figures 9 and 10. On the inbound trajectory, when Galileo approached Jupiter, the dust
543 stream particles (AR1) were mainly detected from rotation angles $270 \pm 70^\circ$ while on the
544 outbound trajectory the streams were detectable from $90 \pm 70^\circ$. Before 2000 the detection
545 geometry of the streams was such that the grains could only be detected during a very
546 limited period of time around perijove passage (Paper VIII, Table 4 therein). This changed
547 in 2000 when the streams became detectable from rotation angles $90 \pm 70^\circ$ during almost
548 the entire orbit of Galileo. This is best seen in orbits G28 to C30 in 2000 and 2001.
549 Big particles were, as in the earlier periods, mostly detected in the inner jovian system
550 when Galileo was close to Jupiter with the exception of several impacts recorded in March
551 2003 at about $350R_J$ from Jupiter (Section 5.4). Note that an error occurred in our earlier
552 rotation angle plots in Paper VIII (Figure 9 in that paper). The corrected figure is shown in
553 the Appendix.

554

Insert Figure 9

555

Insert Figure 10

556 **5 Discussion**

557 The dust data set from Galileo's entire Jupiter mission is a unique set of dust measurements
558 from the jovian system for many years to come. Various jovian dust populations were
559 investigated during the last 15 years which we have summarised in Section 1. The present
560 paper finalises our series of Galileo dust data papers and we discuss some particular aspects
561 of the 2000-2003 data set.

562 **5.1 Variability of Io's dust emission**

563 Imaging observations of Io with Voyager, Galileo, Cassini and New Horizons detected at
564 least 17 volcanic centres with related plumes (Porco et al., 2003; McEwen et al., 2004;
565 Spencer et al., 2007; Geissler and McMillan, 2008). Most of the plumes were sensed

566 through the scattering of sunlight by dust particles entrained within the plumes, and ring-
567 shaped surface deposits on Io suggest that other plumes have been recently active as well.
568 The dust data from the entire Galileo Jupiter mission are a unique record of the dust ejected
569 from Io. In particular, as the plumes are the most plausible sources of the grains (Graps
570 et al., 2000), the dust measurements monitor plume activity (Krüger et al., 2003a).

571 The Galileo dust data show a large orbit-to-orbit variation due to both systematic and
572 stochastic changes. Systematic effects include Io’s orbital motion, changes in the geome-
573 try of Galileo’s orbit and in the magnetic field configuration due to the rotation of Jupiter.
574 Stochastic variations include fluctuations of Io’s volcanic activity, changes of the particle
575 charging in the Io torus, variations in grain release from the torus, and the deformation of
576 the outer magnetosphere in response to the variable solar wind conditions. It should be
577 emphasized that the mechanisms acting on the grains in the Io torus and in particular the
578 connected temporal variability are presently not well understood. By combining the entire
579 Galileo dust data set, the variability due to stochastic processes could be removed and a
580 strong flux variation with jovian local time showed up (Krüger et al., 2003b), confirming
581 earlier predictions (Horányi et al., 1997).

582 Dust emission rates of Io were derived by Krüger et al. (2003a). After removal of the
583 systematic variations, the total dust emission rate of Io turned out to be between 10^{-3} and
584 10 kg s^{-1} , with typical values in the range 0.1 to 1 kg s^{-1} . Exceptionally high dust emission
585 rates occurred during orbits E4 (1996), C21 (1999), G28, and, to a lesser extent, also during
586 G29 and C30. Some of these peaks in the dust emission could be related to specific plume
587 sightings or other markers of volcanic activity on Io: The Pele plume is one of the most
588 powerful plumes and the most steady high-temperature volcanic centre on Io. Surface
589 changes at the Pele site were detected frequently, whereas detections of the Pele plume are
590 relatively rare. Two detections of the Pele plume are coincident with our measurements
591 of high dust fluxes in E4 and G29, while a low dust flux in E6 may be explained by the
592 absence of the Pele plume (McEwen et al., 1998; Porco et al., 2003). In August/September
593 2000 (orbit G28; Section 5.2) when Galileo was far away from Jupiter, a large dust flux
594 was observed which is likely connected with surface changes observed at the site of the
595 Tvashtar plume (Krüger et al., 2003a).

596 Here we investigate the orbit-to-orbit variability of the dust emission pattern on much
597 shorter timescales of days to weeks. As in earlier works (Krüger et al., 2003a) we as-
598 sume a particle radius $s = 10 \text{ nm}$, grain density $\rho = 1.5 \text{ g cm}^{-3}$, dust grain charging to
599 $+5 \text{ V}$ in the Io torus, and calculate the effective dust sensor area from the particle dynamics
600 based on the model of Horányi et al. (1997). We divide the measured dust impact rate by
601 the effective sensor area to obtain the dust flux f ($\text{m}^{-2} \text{ s}^{-1}$) as a function of distance d from
602 Jupiter. If we assume that Io’s dust emission, the dust charging, ejection conditions from
603 the plasma torus and the grain speed remain constant over the time interval considered,
604 we expect a “dilution” of the dust with d^{-2} . Dynamical modelling implies that – after the
605 grains are released from the Io torus – the major acceleration occurs within approximately
606 $10 R_J$ from Jupiter so that their speed remains basically unchanged further away from the
607 planet. Finally, the variation of the dust flux with jovian local time is usually below a factor

608 of five (Krüger et al., 2003b) and thus of minor significance here. With all these assump-
609 tions, we expect a variation of the dust flux with d^{-2} . It should be emphasized that here
610 we use exactly the same assumptions for calculating dust emission rates as Krüger et al.
611 (2003a).

612 **Insert Figure 11**

613 In Table 6 we list the slopes of power law fits $f \propto d^\alpha$ to the derived dust flux profiles. We
614 only considered Galileo orbits where sufficiently long data sets for at least two days are
615 available so that meaningful flux profiles could be obtained. Large variations in the flux
616 profiles are obvious from Table 6. Given the overall uncertainties we believe that slopes in
617 the range $-3 \lesssim \alpha \lesssim -1$ are still compatible with a rather constant dust ejection rate from
618 Io and the Io torus ($\alpha = -2$). In Figure 11 we show the dust flux during the G29 orbit as
619 an example. Here the power law fit to the data gives a slope $\alpha \approx -2$, indicating that the
620 dust release from the Io torus stayed remarkably constant for a rather long period of more
621 than two months.

622 Large deviations from this simple and ideal case with constant dust ejection are also ob-
623 vious in the table. For example, orbits E4, E19, I32 and A34 show very flat profiles in
624 the range $-1 \lesssim \alpha \lesssim 0$, implying that during these orbits stronger dust emissions occurred
625 when Galileo was far away from Jupiter than when the spacecraft was closer to the planet.
626 On the other hand, during orbits G2, G8, E14, E16, E18 and E26 Galileo experienced a
627 stronger dust ejection when the spacecraft was in the inner jovian system (power law slopes
628 $-4 \lesssim \alpha \lesssim -7$). Note that the time coverage of these data sets usually ranges from days to
629 a few weeks, indicating that Io's plume activity or the dust charging and release from the
630 Io torus, or both frequently changed on such rather short timescales.

631 **Insert Table 6**

632 Dust production rates of Io calculated with the method described above are also listed in
633 Table 6. It should be emphasized that within less than a week the dust release frequently
634 changed by approximately a factor of 10, and the absolute levels of the dust emission may
635 have been vastly different from one Galileo orbit to the next. For a detailed discussion of
636 the total dust ejection rates from Io and correlations with individual plume sightings the
637 reader is referred to Krüger et al. (2003a) who showed that all intervals with elevated dust
638 emission exceeding $\sim 1 \text{ kg s}^{-1}$ (six intervals in total) can be connected with giant plume
639 eruptions or large area surface changes on Io or both. See also Section 5.2.

640 **5.2 Io's dust emission in August/September 2000**

641 In summer 2000 (orbit G28) Galileo left the jovian magnetosphere for the first time since it
642 was injected into the jovian system in 1995 and reached a joviocentric distance of $\sim 280R_J$

643 (0.13 AU). In August/September 2000, around Galileo's apojove, the dust instrument mea-
644 sured a surprisingly large dust impact rate exceeding 10 min^{-1} for about two months (Fig-
645 ure 12). Similarly high fluxes were also recorded with the Cassini dust instrument at
646 $\sim 0.3 \text{ AU}$ from Jupiter when the spacecraft was approaching the planet in September 2000
647 (Sascha Kempf, personal communication). The dust emission from Io derived from the
648 Galileo measurements by Krüger et al. (2003a) in this time period exceeds $\sim 100 \text{ kg s}^{-1}$.
649 Later, when Galileo approached Jupiter again, the dust flux profile showed a surprisingly
650 steep drop (slope $\alpha \approx 10$), implying a huge decrease in Io's dust emission.

651 **Insert Figure 12**

652 Frequency analysis of the Galileo dust data from the first three years of the Galileo Jupiter
653 mission (1996-1998) revealed strong 5 and 10 hour periodicities which were due to Jupiter's
654 rotation (Graps et al., 2000). A weak "Io footprint" with approximately 42 hour frequency
655 caused by this moon's orbital motion about Jupiter and harmonics with Jupiter's rotation
656 frequencies were also revealed. These data were collected mostly in the inner jovian mag-
657 netosphere between 10 and $60 R_J$. In the data obtained during the later Galileo orbits
658 in 1999 and 2000 the Io footprint became more prominent and was evident during most
659 Galileo orbits from E19 to G29 (Graps, 2001).

660 In the data from a total of 26 Galileo orbits measured between 1996 and 2000, a total of
661 11 orbits showed a clear modulation with Io's frequency, 3 showed a weak Io modulation,
662 while the remaining 12 orbits showed no Io signature at all (Graps, 2001). In many, but
663 not all, cases the missing Io signature coincided with time periods when a rather weak dust
664 flux was measured.

665 In the data set from August/September 2000, collected between days 00-220 and 00-250
666 at much larger jovicentric distances, Io's signature dominated all other frequency signa-
667 tures including the 5 and 10 hour periods caused by Jupiter's rotation (Graps et al., 2001).
668 These data provide direct evidence for Io being the source for the majority of the jovian
669 dust stream particles during this time period. The presence of Io's orbital frequency im-
670 plies that Io is a localised source of charged dust particles because charged dust from dif-
671 fuse sources would couple to Jupiter's magnetic field and appear in frequency space with
672 Jupiter's rotation frequency and its harmonics.

673 The period of strong dust emission seen in August/September 2000 coincided with en-
674 hanced neutral gas production from the Io torus, suggesting a coupling mechanism between
675 gas and dust ejection, although the relation between the dust emissions and the production
676 of neutral gas is not known (Delamere et al., 2004). Furthermore, there was a significant
677 reduction in the neutral source beginning in October 2000, again coinciding with the strong
678 drop in the dust emission as derived from our Galileo dust data.

679 **5.3 Galileo-Cassini joint dust stream measurements**

680 On 30 December 2000 the Cassini spacecraft flew by Jupiter, providing a unique oppor-
681 tunity for a two-spacecraft time-of-flight measurement (Cassini-Galileo) of particles from

682 one collimated stream from the jovian dust streams. The goal was to detect particles in a
683 stream first with Galileo when the spacecraft was inside the jovian magnetosphere close
684 to the orbit of Europa (about $12R_J$), and particles in potentially the same stream later by
685 Cassini outside the magnetosphere (at $140R_J$) (see Graps et al., 2001, for a preliminary
686 analysis).

687 The Cassini data from the Jupiter flyby imply that particles of different sizes have different
688 phases with respect to Jupiter's rotation (Sascha Kempf, personal communication), a result
689 which is also seen in earlier Galileo data (Grün et al., 1998). Comparison of the measure-
690 ments from both dust instruments, however, is hampered by the higher detection sensitivity
691 of the Cassini detector with respect to the Galileo sensor. Both instruments have detected
692 stream particles with different sizes and, hence likely different phases. The analysis is
693 ongoing (Hsiang-Wen Hsu, personal communication), and more detailed modelling to de-
694 scribe the phase relation of different-sized particles taking into account the 3-dimensional
695 structure of the dust emission pattern from the jovian system is necessary. Our present
696 preliminary analysis indicates particle speeds of about 400 km s^{-1} . This value is in agree-
697 ment with speeds for 10 nm particles as derived from dynamical modelling (Hamilton and
698 Burns, 1993; Horányi et al., 1993), and earlier studies of the jovian dust stream dynamics
699 (Zook et al., 1996).

700 **5.4 Large dust grains far from Jupiter**

701 On 29 December 2002 (day 02-363) the last MRO of the dust instrument memory occurred
702 for the remainder of the Galileo mission. The next time we received dust data was during
703 the time interval 4 to 11 March 2003 (days 03-063 to 03-070). These data were obtained as
704 RTS data. We identified a total number of nine large dust impacts in amplitude ranges AR2-
705 4 which occurred between 29 December 2002 and 11 March 2003. Due to corruption of the
706 readings from the instrument's internal clock and one clock reset in this time interval, two
707 of these impacts have an exceptionally large uncertainty in the impact time of 66 days. We
708 could reconstruct the impact time of the remaining seven impacts with a higher accuracy
709 from accumulator readings obtained with test pulses which were routinely performed by
710 the dust instrument (see Krüger et al., 2005, for more details). This gave impact times for
711 five impacts with about one day uncertainty and for two impacts with 4.3 hour uncertainty
712 (Table 7).

713 The reconstruction of these partially corrupted data implies that at least seven impacts oc-
714 curred during a period of only four days when Galileo was outside Jupiter's magnetosphere
715 in interplanetary space at approximately $350R_J$ from Jupiter. This is a surprisingly large
716 number of impacts at such a large distance from Jupiter given the Galileo measurements
717 from the earlier Jupiter mission (Papers VI and VIII) and from Galileo's interplanetary
718 cruise. Potential sources for these grains are, for example, collisional ejecta from an (un-
719 known) small jovian satellite or a cometary trail crossed by the spacecraft. Judging from
720 the impact charge distribution of the measured grains, jovian stream particles (Figure 6)
721 can be most likely ruled out because a much larger number of impacts should have oc-

722 curred in the lower amplitude range AR1. In fact, only few impacts were recognized in
723 AR1 during this time. A more detailed analysis of these impacts has to be postponed to a
724 future investigation.

725 **5.5 Galileo's gossamer ring passages**

726 On 5 November 2002 (orbit A34, day 02-309) Galileo traversed Jupiter's gossamer rings
727 for the first time and approached the planet to $2R_J$. During this ring passage the spacecraft
728 had a close flyby at Amalthea at 244 km distance from the moon's centre, well outside
729 Amaltheas's Hill sphere. During approach to Jupiter dust data were collected with the
730 highest possible rate (record mode; Section 2.3) while Galileo was within Io's orbit (i.e.
731 within $\sim 5.9R_J$). Shortly after Amalthea flyby a spacecraft anomaly at $2.33R_J$ jovicentric
732 distance prevented the collection of further Galileo dust data. Although the dust instrument
733 continued to measure dust impacts after the anomaly, the data were not written to the tape
734 recorder on board and, hence, the majority of them were lost. Only the data sets of a few
735 dust impacts were received from an MRO on day 02-322. These events could be located to
736 have happened during the gossamer ring passage but their impact time is uncertain by a few
737 hours (Table 7). The traverse of the optically visible ring from its outer edge at $\sim 3.75R_J$
738 until the spacecraft anomaly occurred lasted about 100 min, and the total gossamer ring
739 traverse from $\sim 3.75R_J$ inbound to $\sim 3.75R_J$ outbound took approximately six hours.

740 During the A34 ring passage the lowest amplitude range in class 2 (AC21) was strongly
741 contaminated with noise, while the higher amplitude ranges showed little or no noise con-
742 tamination. In addition, many class 1 events recognised within Io's orbit showed signatures
743 of being true dust impacts as well. The noise identification scheme applied to the dust data
744 from both Galileo gossamer ring passages is described in Section 3.1 and given in Table 5.

745 With the new noise identification scheme, complete data sets of 90 dust impacts were
746 identified in the Galileo recorded data from the gossamer ring region. Several hundred
747 more events were counted only and their data sets were lost, in particular in AR1. The
748 completeness of the transmitted ring data varied between 100% in the highest amplitude
749 ranges (AR2-4) in the faint ring extension beyond Thebe's orbit down to only 4% for the
750 lowest amplitude range (AR1) in the more populated Amalthea ring.

751 In record mode, the dust instrument memory was read out once per minute, and this read-
752 out frequency determined the spatial resolution of the measurements: within one minute
753 Galileo moved about 1,800 km through the ring which corresponds to about 1,100 km (or
754 $0.015R_J$) in radial direction. This is the highest spatial resolution achievable in the ring
755 with the Galileo in-situ measurements.

756 Dust measurements in the gossamer rings were also obtained during Galileo's second ring
757 traverse on 21 September 2003 (orbit J35) a few hours before Galileo impacted Jupiter.
758 The data sets of about 20 dust impacts were successfully transmitted to Earth as RTS data.
759 This time the spatial resolution was only about 14,000 km (or $0.2R_J$).

760 The data from both gossamer ring traverses allowed for the first actual comparison of in-

761 situ measurements with the properties inferred from inverting optical images. A detailed
762 analysis of this data was published by Krüger et al. (2009). Below we summarise the most
763 important results.

764 Images of the rings imply inclinations of the grain orbits of $i \approx 1^\circ$ for the visible 5 to
765 $10\mu\text{m}$ grains (Showalter et al., 2008). The expected rotation angle for ring particles on
766 circular prograde uninclined joventric orbits was $\simeq 90^\circ$. The rotation angles measured
767 within Io's orbit and in particular during the ring passages were – to a first approximation
768 – consistent with these expectations. However, the width of the rotation angle distribution
769 was much wider than the expected width for the geometry conditions during both gossamer
770 ring passages.

771 What was the reason for such a broad distribution in impact directions? One possibility was
772 the sensor side wall which was very sensitive to dust impacts (Altobelli et al., 2004; Willis
773 et al., 2005). Taking the sensor side wall into account (Table 3), the expected width in
774 rotation angle was still significantly smaller than the observed width. Another potential ex-
775 planation was impacts onto nearby spacecraft structures like the magnetometer boom, the
776 EPD and PLS instruments which masquerade as particles with high inclinations. We are
777 convinced that such an explanation can be ruled out for two reasons (Moissl, 2005): First,
778 the impact parameters (charge rise times, charge signal coincidences, etc.) of grains mea-
779 sured with rotation angles outside the nominal field-of-view for low-inclination particles do
780 not show significant differences compared to gains inside the nominal field-of-view. Sec-
781 ond, the data from both Galileo ring traverses show similarly broad rotation angle patterns
782 although they had different detection geometries. During the first flyby the magnetome-
783 ter boom obscured the field-of-view while during the second flyby this was not the case
784 (Krüger et al., 2009).

785 The most likely explanation for the observed structure in the rotation angle pattern is the
786 particle dynamics: The wide range in impact directions as well as a drop measured in
787 the impact rate profile immediately interior to Thebe's orbit and a gradual increase in the
788 relative abundance of small particles closer to Jupiter can best be explained by a shadow
789 resonance caused by varying particle charge on the day and night side of Jupiter, driving
790 particles onto high inclination orbits (Hamilton and Krüger, 2008). In fact, inclinations up
791 to 20° nicely explain the measured impact directions for most grains.

792 Comparison of our in-situ measurements with imaging observations showed that the in-situ
793 measurements preferentially probe the large population of small sub-micron particles while
794 the images are sensitive to larger grains with radii of at least several microns. The grains
795 form a halo of material faint enough to be invisible to imaging, but populated enough to be
796 detectable with the Galileo sensor. The faint gossamer ring extension previously imaged
797 to about $3.75R_J$ was detected out to at least $5R_J$, indicating that ejecta from Thebe spread
798 much further and particle orbits get higher eccentricities than previously known. Both the
799 gap in the ring and the faint ring extension indicate that the grain dynamics is strongly
800 influenced by electromagnetic forces. For a more detailed discussion of the ring particle
801 dynamics the reader is referred to Hamilton and Krüger (2008).

6 Conclusions

In this paper, which is the tenth in a series of Galileo and Ulysses dust data papers, we present data from the Galileo dust instrument for the period January 2000 to September 2003. In this time interval the spacecraft completed nine revolutions about Jupiter in the joviocentric distance range between 2 and $370R_J$ (Jupiter radius, $R_J = 71,492\text{ km}$). On 21 September 2003 Galileo was destroyed in a planned impact with Jupiter.

The data sets of a total of 5389 (or 2% of the total) recorded dust impacts were transmitted to Earth in this period. Many more impacts (98%) were counted with the accumulators of the instrument but their complete information was lost because of the low data transmission capability of the Galileo spacecraft. Together with 15861 impacts recorded in interplanetary space and in the Jupiter system between Galileo's launch in October 1989 and December 1999 published earlier (Grün et al., 1995a; Krüger et al., 1999a, 2001a, 2006b), the complete data set of dust impacts measured with the dust detector during Galileo's entire mission contains 21250 impacts.

Galileo has been an extremely successful dust detector, measuring dust streams flowing away from Jupiter, a tenuous dust ring throughout the jovian magnetosphere and Jupiter's gossamer rings over the almost four year timespan of data considered in this paper.

Most of the time the jovian dust streams dominated the overall impact rate, reaching maxima of more than 10 min^{-1} in the inner jovian system. A surprisingly large impact rate up to 100 min^{-1} was measured in August/September 2000 (G28 orbit) when the spacecraft was at about $280R_J$ distance from Jupiter. This strong dust emission was most likely connected with a heavy volcanic eruption on Io (Krüger et al., 2003a; Geissler, 2003; Geissler et al., 2004). A strong variation in the release of neutral gas from the Io torus in this time interval was also reported by Delamere et al. (2004).

Io's dust emission as derived from the measured dust fluxes varied by many orders of magnitude, with typical values ranging between 0.01 to 1 kg s^{-1} of dust ejected. In August/September 2000 the derived dust emission exceeded 100 kg s^{-1} . The investigation of the dust impact rate profiles measured for the jovian stream particles as a function of radial distance from Jupiter revealed large orbit-to-orbit variations and variability by a factor of 10 or more on timescales of days to a few weeks. This implies strong variability of the dust release from Io or the Io torus or variability of the jovian magnetosphere on such short timescales.

A surprisingly large number of impacts of bigger micron-sized dust grains was detected within a 4-day time interval far away from Jupiter in March 2003 when Galileo was in interplanetary space. The source of these grains remains unclear.

Finally, in November 2002 and September 2003 Galileo traversed Jupiter's gossamer rings twice, providing the first actual opportunity to compare in-situ dust measurements with the results obtained from remote imaging. These flybys revealed previously unknown structures in the gossamer rings (Krüger et al., 2009): a drop in the dust density between the moons Amalthea and Thebe, grains orbiting Jupiter on highly inclined orbits and an increase in the number of small grains in the inner regions of the rings as compared to the

843 regions further away from the planet. All these features can nicely be explained by electro-
844 magnetic forces on the grains that shape the gossamer rings (Hamilton and Krüger, 2008).
845 Strong degradation of the dust instrument electronics was recognised in the Galileo dust
846 data (Krüger et al., 2005). It was most likely caused by the harsh radiation environment
847 in the jovian magnetosphere and lead to a degradation of the instrument sensitivity for
848 noise and dust detection during the Galileo mission. The Galileo data set obtained until
849 the end of 1999 (Papers VI and VIII) was not seriously affected by this degradation. In
850 the time interval 2000 to 2003 which is the subject of this paper, however, the electronics
851 degradation became so severe that the instrument calibration does not give reliable impact
852 speeds and masses of the dust particles anymore. Instead, only lower limits for the impact
853 speed and upper limits for the grain mass, respectively, can be given. The only exception
854 are dust impacts for which their impact speeds can be derived from other means (e.g.
855 impacts in the gossamer rings; Krüger et al., 2009). On the other hand, a reduction of
856 the channeltron amplification was counterbalanced by four increases of the channeltron
857 high voltage during the entire Jupiter mission (two in 1999, one each in 2000 and 2001) to
858 maintain stable instrument operation.

859 Even though this is the final paper in our series of Galileo dust data papers published
860 during the last 15 years, the evaluation of this unique data set is continuing. A list of
861 specific open questions raised in this and earlier data papers includes:

- 862 • *Electromagnetic interaction and phase relation of different sized stream particles:*
863 Dust grains with different sizes have a different susceptibility to electromagnetic
864 interaction with the jovian magnetosphere. Different-sized grains released from a
865 source in the inner jovian system at the same time are expected to arrive at Galileo at
866 a different phase of Jupiter's rotation (Grün et al., 1998). This rather simple picture
867 is further complicated by the grains' charging history. Studies of the phase relation
868 may lead to better constraints of the grain size distribution and may give new insights
869 into the grains' electromagnetic interaction. The phase relation may turn out to be
870 essential to understand the Galileo-Cassini joint dust streams measurements.
- 871 • *Galileo-Cassini joint dust streams measurements:* Being originally designed as a
872 two-spacecraft time-of-flight measurement of one collimated stream from the jovian
873 dust streams, the analysis of this data set turned out to be more complicated than an-
874 ticipated. More detailed modelling of the 3-dimensional structure of the dust stream
875 emission pattern from the jovian system is necessary to describe the phase relation
876 of different-sized particles and to understand these unique measurements.
- 877 • *"Big" micron-sized particles:* Impacts of micron-sized dust grains were preferen-
878 tially detected in the inner jovian system between the Galilean moons. Two sub-
879 populations – one orbiting Jupiter on prograde and one on retrograde orbits – were
880 identified in earlier analyses (Thiessenhusen et al., 2000). The derived ratio in num-
881 ber density was approximately 4:1 with the majority of grains being on prograde
882 orbits. At the time, however, only about half of the entire Galileo dust data set

883 from Jupiter was available. Given that the detection geometry of the dust instrument
884 changed with time during the mission, re-evaluation of the full data set from the en-
885 tire Galileo Jupiter mission would be worthwhile to verify the abundance of grains
886 on retrograde orbits.

- 887 • *Dust-plasma interaction:* Very preliminary comparison of the Galileo dust measure-
888 ments from the gossamer ring passages with energetic particle data from the same
889 period has revealed some interesting correlations between both data sets (Norbert
890 Krupp, personal communication). New insights into the dust-plasma interaction and
891 particle dynamics can be expected from combined studies of the dust data and other
892 Galileo particles and fields data.

893

894 **Acknowledgements.** We dedicate this work to the memory of Dietmar Linkert who passed
895 away in spring 2009. He was Principal Engineer for space instruments at MPI für Kern-
896 physik including the dust instruments flown on the HEOS-2, Helios, Galileo, Ulysses and
897 Cassini missions. His friends and colleagues around the world appreciated his experi-
898 ence and sought his professional advice. The authors wish to thank the Galileo project at
899 NASA/JPL for effective and successful mission operations. This research was supported
900 by the German Bundesministerium für Bildung und Forschung through Deutsches Zentrum
901 für Luft- und Raumfahrt e.V. (DLR, grant 50 QJ 9503 3). Support by MPI für Kernphysik
902 and MPI für Sonnensystemforschung is also gratefully acknowledged.

903 **ERRATUM**

904 Due to an error in Paper VIII, all panels of Figure 9 in that paper have wrong labels on the
905 vertical axis. Furthermore, the third panel (data of 1999) erroneously shows the dataset of
906 1997. We apologize for this error and show the corrected plots in Figure 13.

907

Insert Figure 13

References

- 908
- 909 Altobelli, N., Moissl, R., Krüger, H., Landgraf, M., and Grün, E. (2004). Influence of wall
910 impacts on the Ulysses dust detector in modelling the interstellar dust flux. *Planetary
911 and Space Science*, 52:1287–1295.
- 912 Anderson, J. D., Johnson, T. V., Schubert, G., Asmar, S., Jacobson, R. A., Johnston, D.,
913 Lau, E. L., Lewis, G., Moore, W. B., Taylor, A., Thomas, P. C., and Weinwurm, G.
914 (2005). Amalthea’s Density Is Less Than That of Water. *Science*, 308:1291–1293.
- 915 Colwell, J. E., Horányi, M., and Grün, E. (1998). Capture of interplanetary and interstellar
916 dust by the Jovian magnetosphere. *Science*, 280:88–91.
- 917 D’Amario, L. A., Bright, L. E., and Wolf, A. A. (1992). Galileo trajectory design. *Space
918 Science Reviews*, 60:23–78.
- 919 Delamere, P. A., Steffl, A., and Bagenal, F. (2004). Modeling temporal variability of
920 plasma conditions in the Io torus during the Cassini era. *Journal of Geophysical Re-
921 search (Space Physics)*, 109:10216–10224.
- 922 Flandes, A. (2005). *Dust dynamics in the jovian system*. PhD thesis, Universidad Nacional
923 Autonoma de Mexico.
- 924 Flandes, A. and Krüger, H. (2007). Solar wind modulation of Jupiter dust stream detection.
925 In H. Krüger and A. L. Graps, editor, *Dust in planetary systems*, pages 87–90. ESA SP-
926 643.
- 927 Flandes, A., Krüger, H., Hamilton, D. P., and Valdés-Galicia, J. F. (2009). Magnetic field
928 modulated dust streams from Jupiter in interplanetary space. *Icarus*. in preparation.
- 929 Geissler, P. E. (2003). Volcanic Activity on Io During the Galileo Era. *Annual Reviews of
930 Earth and Planetary Sciences*, 31:175–211.
- 931 Geissler, P. E., McEwen, A., Phillips, C., Kesthelyi, L., and Spencer, J. (2004). Surface
932 Changes on Io during the Galileo Mission. *Icarus*, 169:29–64.
- 933 Geissler, P. E. and McMillan, M. T. (2008). Galileo observations of volcanic plumes on Io.
934 *Icarus*, 197:505–518.
- 935 Graps, A. L. (2001). *Io revealed in the Jovian dust streams*. PhD thesis, Ruprecht-Karls-
936 Universität Heidelberg.
- 937 Graps, A. L. (2006). Characterization of Jovian plasma-embedded dust particles. *Planetary
938 and Space Science*, 54:911–918.
- 939 Graps, A. L., Grün, E., Krüger, H., Horányi, M., and Svedhem, H. (2001). Io revealed
940 in the jovian dust streams. In *Proceedings of the Meteoroids 2001 Conference, ESA
941 SP-495*, pages 601–608.

- 942 Graps, A. L., Grün, E., Svedhem, H., Krüger, H., Horányi, M., Heck, A., and Lammers, S.
943 (2000). Io as a source of the Jovian dust streams. *Nature*, 405:48–50.
- 944 Grün, E., Baguhl, M., Divine, N., Fechtig, H., Hamilton, D. P., Hanner, M. S., Kissel,
945 J., Lindblad, B. A., Linkert, D., Linkert, G., Mann, I., McDonnell, J. A. M., Morfill,
946 G. E., Polanskey, C., Riemann, R., Schwehm, G. H., Siddique, N., Staubach, P., and
947 Zook, H. A. (1995a). Three years of Galileo dust data. *Planetary and Space Science*,
948 43:953–969. Paper II.
- 949 Grün, E., Baguhl, M., Divine, N., Fechtig, H., Hamilton, D. P., Hanner, M. S., Kissel,
950 J., Lindblad, B. A., Linkert, D., Linkert, G., Mann, I., McDonnell, J. A. M., Morfill,
951 G. E., Polanskey, C., Riemann, R., Schwehm, G. H., Siddique, N., Staubach, P., and
952 Zook, H. A. (1995b). Two years of Ulysses dust data. *Planetary and Space Science*,
953 43:971–999. Paper III.
- 954 Grün, E., Baguhl, M., Hamilton, D. P., Kissel, J., Linkert, D., Linkert, G., and Riemann,
955 R. (1995c). Reduction of Galileo and Ulysses dust data. *Planetary and Space Science*,
956 43:941–951. Paper I.
- 957 Grün, E., Baguhl, M., Hamilton, D. P., Riemann, R., Zook, H. A., Dermott, S. F., Fechtig,
958 H., Gustafson, B. A., Hanner, M. S., Horányi, M., Khurana, K. K., Kissel, J., Kivelson,
959 M., Lindblad, B. A., Linkert, D., Linkert, G., Mann, I., McDonnell, J. A. M., Morfill,
960 G. E., Polanskey, C., Schwehm, G. H., and Srama, R. (1996a). Constraints from Galileo
961 observations on the origin of Jovian dust streams. *Nature*, 381:395–398.
- 962 Grün, E., Fechtig, H., Hanner, M. S., Kissel, J., Lindblad, B. A., Linkert, D., Maas, D.,
963 Morfill, G. E., and Zook, H. A. (1992a). The Galileo dust detector. *Space Science*
964 *Reviews*, 60:317–340.
- 965 Grün, E., Fechtig, H., Kissel, J., Linkert, D., Maas, D., McDonnell, J. A. M., Morfill, G. E.,
966 Schwehm, G. H., Zook, H. A., and Giese, R. H. (1992b). The Ulysses dust experiment.
967 *Astronomy and Astrophysics, Supplement*, 92:411–423.
- 968 Grün, E., Hamilton, D. P., Riemann, R., Dermott, S. F., Fechtig, H., Gustafson, B. A.,
969 Hanner, M. S., Heck, A., Horányi, M., Kissel, J., Kivelson, M., Krüger, H., Lindblad,
970 B. A., Linkert, D., Linkert, G., Mann, I., McDonnell, J. A. M., Morfill, G. E., Polanskey,
971 C., Schwehm, G. H., Srama, R., and Zook, H. A. (1996b). Dust measurements during
972 Galileo’s approach to Jupiter and Io encounter. *Science*, 274:399–401.
- 973 Grün, E., Krüger, H., Graps, A., Hamilton, D. P., Heck, A., Linkert, G., Zook, H., Dermott,
974 S. F., Fechtig, H., Gustafson, B., Hanner, M., Horányi, M., Kissel, J., Lindblad, B.,
975 Linkert, G., Mann, I., McDonnell, J. A. M., Morfill, G. E., Polanskey, C., Schwehm,
976 G. H., and Srama, R. (1998). Galileo observes electromagnetically coupled dust in the
977 Jovian magnetosphere. *Journal of Geophysical Research*, 103:20011–20022.

- 978 Grün, E., Krüger, P., Dermott, S. F., Fechtig, H., Graps, A. L., Gustafson, B. A., Hamilton,
979 D. P., Heck, A., Horányi, M., Kissel, J., Lindblad, B. A., Linkert, D., Linkert, G., Mann,
980 I., McDonnell, J. A. M., Morfill, G. E., Polanskey, C., Schwehm, G. H., Srama, R., and
981 Zook, H. A. (1997a). Dust measurements in the Jovian magnetosphere. *Geophysical
982 Research Letters*, 24:2171–2174.
- 983 Grün, E., Staubach, P., Baguhl, M., Hamilton, D. P., Zook, H. A., Dermott, S. F., Gustafson,
984 B. A., Fechtig, H., Kissel, J., Linkert, D., Linkert, G., Srama, R., Hanner, M. S.,
985 Polanskey, C., Horányi, M., Lindblad, B. A., Mann, I., McDonnell, J. A. M., Mor-
986 fill, G. E., and Schwehm, G. H. (1997b). South-North and Radial Traverses through the
987 Interplanetary Dust Cloud. *Icarus*, 129:270–288.
- 988 Grün, E., Zook, H. A., Baguhl, M., Balogh, A., Bame, S. J., Fechtig, H., Forsyth, R.,
989 Hanner, M. S., Horányi, M., Kissel, J., Lindblad, B. A., Linkert, D., Linkert, G., Mann,
990 I., McDonnell, J. A. M., Morfill, G. E., Phillips, J. L., Polanskey, C., Schwehm, G. H.,
991 Siddique, N., Staubach, P., Svestka, J., and Taylor, A. (1993). Discovery of Jovian dust
992 streams and interstellar grains by the Ulysses spacecraft. *Nature*, 362:428–430.
- 993 Hamilton, D. P. and Burns, J. A. (1993). Ejection of dust from Jupiter’s gossamer ring.
994 *Nature*, 364:695–699.
- 995 Hamilton, D. P. and Krüger, H. (2008). Jupiter’s shadow sculpts its gossamer rings. *Nature*,
996 453:72–75.
- 997 Heck, A. (1998). *Modellierung und Analyse der von der Raumsonde Galileo im Jupiter-
998 system vorgefundenen Mikrometeoroiden-Populationen*. PhD thesis, Ruprecht-Karls-
999 Universität Heidelberg.
- 1000 Horányi, M., Grün, E., and Heck, A. (1997). Modeling the Galileo dust measurements at
1001 Jupiter. *Geophysical Research Letters*, 24:2175–2178.
- 1002 Horányi, M., Morfill, G. E., and Grün, E. (1993). Mechanism for the acceleration and
1003 ejection of dust grains from Jupiter’s magnetosphere. *Nature*, 363:144–146.
- 1004 Johnson, T. V., Yeates, C., and Young, R. (1992). Galileo Mission Overview. *Space Science
1005 Reviews*, 60:3–21.
- 1006 Kempf, S., Beckmann, U., Srama, R., Horanyi, M., Auer, S., and Grün, E. (2006). The
1007 electrostatic potential of E ring particles. *Planetary and Space Science*, 54:999–1006.
- 1008 Kempf, S., Srama, R., Altobelli, N., Auer, S., Tschernjawski, V., Bradley, J., Burton,
1009 M. E., Helfert, S., Johnson, T. V., Krüger, H., Moragas-Klostermeyer, G., and Grün, E.
1010 (2004). Cassini between Earth and asteroid belt: first in-situ charge measurements of
1011 interplanetary grains. *Icarus*, 171:317–335.

- 1012 Krivov, A. V., Krüger, H., Grün, E., Thiessenhusen, K.-U., and Hamilton, D. P. (2002a).
1013 A tenuous dust ring of Jupiter formed by escaping ejecta from the Galilean satellites.
1014 *Journal of Geophysical Research*, 107:E1, 10.1029/2000JE001434.
- 1015 Krivov, A. V., Sremčević, M., Spahn, F., Dikarev, V. V., and Kholshchevnikov, K. V. (2003).
1016 Impact-generated dust clouds around planetary satellites: Spherically-symmetric case.
1017 *Planetary and Space Science*, 51:251–269.
- 1018 Krivov, A. V., Wardinski, I., Spahn, F., Krüger, H., and Grün, E. (2002b). Dust on the
1019 outskirts of the Jovian system. *Icarus*, 157:436–455.
- 1020 Krüger, H., Hamilton, D. P., Moissl, R., and Grün, E. (2009). Galileo in-situ dust measure-
1021 ments in Jupiter’s gossamer rings. *Icarus*. in press.
- 1022 Krüger, H. (2003). *Jupiter’s Dust Disc, An Astrophysical Laboratory*. Shaker Verlag
1023 Aachen, ISBN 3-8322-2224-3. Habilitation Thesis Ruprecht-Karls-Universität Heidel-
1024 berg.
- 1025 Krüger, H., Altobelli, N., Anweiler, B., Dermott, S. F., Dikarev, V., Graps, A. L., Grün,
1026 E., Gustafson, B. A., Hamilton, D. P., Hanner, M. S., Horányi, M., Kissel, J., Landgraf,
1027 M., Lindblad, B., Linkert, D., Linkert, G., Mann, I., McDonnell, J. A. M., Morfill, G. E.,
1028 Polanskey, C., Schwehm, G. H., Srama, R., and Zook, H. A. (2006a). Five years of
1029 Ulysses dust data: 2000 to 2004. *Planetary and Space Science*, 54:932–956. Paper IX.
- 1030 Krüger, H., Bindschadler, D., Dermott, S. F., Graps, A. L., Grün, E., Gustafson, B. A.,
1031 Hamilton, D. P., Hanner, M. S., Horányi, M., Kissel, J., Lindblad, B., Linkert, D.,
1032 Linkert, G., Mann, I., McDonnell, J. A. M., Moissl, R., Morfill, G. E., Polanskey, C.,
1033 Schwehm, G. H., Srama, R., and Zook, H. A. (2006b). Galileo dust data from the jovian
1034 system: 1997 to 1999. *Planetary and Space Science*, 54:879–910. Paper VIII.
- 1035 Krüger, H., Dikarev, V., Anweiler, B., Dermott, S. F., Graps, A. L., Grün, E., Gustafson,
1036 B. A., Hamilton, D. P., Hanner, M. M. S., Horányi, M., Kissel, J., Linkert, D., Linkert,
1037 G., Mann, I., McDonnell, J. A. M., Morfill, G. E., Polanskey, C., Schwehm, G. H., and
1038 Srama, R. (2010). Three years of Ulysses dust data: 2005 to 2007. *Planetary and Space
1039 Science*. Paper XI, submitted.
- 1040 Krüger, H., Geissler, P., Horányi, M., Graps, A. L., Kempf, S., Srama, R., Moragas-
1041 Klostermeyer, G., Moissl, R., Johnson, T. V., and Grün, E. (2003a). Jovian dust streams:
1042 A Monitor of Io’s volcanic plume activity. *Geophysical Research Letters*, 30:2101–2105.
- 1043 Krüger, H., Graps, A. L., Hamilton, D. P., Flandes, A., Forsyth, R. J., Horányi, M., and
1044 Grün, E. (2006c). Ulysses jovian latitude scan of high-velocity dust streams originating
1045 from the jovian system. *Planetary and Space Science*, 54:919–931.
- 1046 Krüger, H., Grün, E., Graps, A. L., Bindschadler, D. L., Dermott, S. F., Fechtig, H.,
1047 Gustafson, B. A., Hamilton, D. P., Hanner, M. S., Horányi, M., Kissel, J., Lindblad,

- 1048 B., Linkert, D., Linkert, G., Mann, I., McDonnell, J. A. M., Morfill, G. E., Polanskey,
1049 C., Schwehm, G. H., Srama, R., and Zook, H. A. (2001a). One year of Galileo dust data
1050 from the jovian system: 1996. *Planetary and Space Science*, 49:1285–1301. Paper VI.
- 1051 Krüger, H., Grün, E., Hamilton, D. P., Baguhl, M., Dermott, S. F., Fechtig, H., Gustafson,
1052 B. A., Hanner, M. S., Horányi, M., Kissel, J., Lindblad, B. A., Linkert, D., Linkert, G.,
1053 Mann, I., McDonnell, J. A. M., Morfill, G. E., Polanskey, C., Riemann, R., Schwehm,
1054 G. H., Srama, R., and Zook, H. A. (1999a). Three years of Galileo dust data: II. 1993 to
1055 1995. *Planetary and Space Science*, 47:85–106. Paper IV.
- 1056 Krüger, H., Grün, E., Heck, A., and Lammers, S. (1999b). Analysis of the sensor character-
1057 istics of the Galileo dust detector with collimated Jovian dust stream particles. *Planetary
1058 and Space Science*, 47:1015–1028.
- 1059 Krüger, H., Grün, E., Landgraf, M., Baguhl, M., Dermott, S. F., Fechtig, H., Gustafson,
1060 B. A., Hamilton, D. P., Hanner, M. S., Horányi, M., Kissel, J., Lindblad, B., Linkert,
1061 D., Linkert, G., Mann, I., McDonnell, J. A. M., Morfill, G. E., Polanskey, C., Schwehm,
1062 G. H., Srama, R., and Zook, H. A. (1999c). Three years of Ulysses dust data: 1993 to
1063 1995. *Planetary and Space Science*, 47:363–383. Paper V.
- 1064 Krüger, H., Grün, E., Landgraf, M., Dermott, S. F., Fechtig, H., Gustafson, B. A., Hamil-
1065 ton, D. P., Hanner, M. S., Horányi, M., Kissel, J., Lindblad, B., Linkert, D., Linkert, G.,
1066 Mann, I., McDonnell, J. A. M., Morfill, G. E., Polanskey, C., Schwehm, G. H., Srama,
1067 R., and Zook, H. A. (2001b). Four years of Ulysses dust data: 1996 to 1999. *Planetary
1068 and Space Science*, 49:1303–1324. Paper VII.
- 1069 Krüger, H., Grün, E., Linkert, D., Linkert, G., and Moissl, R. (2005). Galileo long-term
1070 dust monitoring in the jovian magnetosphere. *Planetary and Space Science*, 53:1109–
1071 1120.
- 1072 Krüger, H., Horányi, M., and Grün, E. (2003b). Jovian dust streams: Probes of the Io
1073 plasma torus. *Geophysical Research Letters*, 30:1058–1061.
- 1074 Krüger, H., Horányi, M., Krivov, A. V., and Graps, A. L. (2004). *Jovian dust:
1075 streams, clouds and rings*, pages 219–240. Jupiter. The planet, satellites and magne-
1076 tosphere. Edited by Fran Bagenal, Timothy E. Dowling, William B. McKinnon. Cam-
1077 bridge planetary science, Vol. 1, Cambridge, UK: Cambridge University Press, ISBN
1078 0-521-81808-7, 2004.
- 1079 Krüger, H., Krivov, A. V., and Grün, E. (2000). A dust cloud of Ganymede maintained by
1080 hypervelocity impacts of interplanetary micrometeoroids. *Planetary and Space Science*,
1081 48:1457–1471.
- 1082 Krüger, H., Krivov, A. V., Hamilton, D. P., and Grün, E. (1999d). Detection of an impact-
1083 generated dust cloud around Ganymede. *Nature*, 399:558–560.

- 1084 Krüger, H., Krivov, A. V., Sremčević, M., and Grün, E. (2003c). Galileo measurements of
1085 impact-generated dust clouds surrounding the Galilean satellites. *Icarus*, 164:170–187.
- 1086 McEwen, A., Keszthelyi, L., Lopes, R., Schenk, P., and Spencer, J. (2004). The Litho-
1087 sphere and Surface of Io. In Bagenal, F., McKinnon, B., and Dowling, T., editors,
1088 *Jupiter: Planet, Satellites & Magnetosphere*, pages 307–328. Cambridge University
1089 Press.
- 1090 McEwen, A. S., Keszthelyi, L., Geissler, P., Simonelli, D. P., Carr, M. H., Johnson, T. V.,
1091 Klaasen, K. P., Breneman, H. H., Jones, T. J., Kaufman, J. M., Magee, K. P., Senske,
1092 D. A., Belton, M. J. S., and Schubert, G. (1998). Active volcanism on Io as seen by
1093 Galileo SSI. *Icarus*, 135:181–219.
- 1094 Moissl, R. (2005). *Galileos Staubmessungen in Jupiters Gossamer-Ringen*. Ruprecht-
1095 Karls-Universität Heidelberg. Diplom thesis.
- 1096 Porco, C. C., West, R. A., McEwen, A., Del Genio, A. D., Ingersoll, A. P., Thomas, P.,
1097 Squyres, S., Dones, L., Murray, C. D., Johnson, T. V., Burns, J. A., Brahic, A., Neukum,
1098 G., Veverka, J., Barbara, J. M., Denk, T., Evans, M., Ferrier, J. J., Geissler, P., Helfen-
1099 stein, P., Roatsch, T., Throop, H., Tiscareno, M., and Vasavada, A. R. (2003). Cassini
1100 Imaging of Jupiter’s Atmosphere, Satellites, and Rings. *Science*, 299:1541–1547.
- 1101 Postberg, F., Kempf, S., Green, S. F., Hillier, J. K., McBride, N., and Grün, E. (2006).
1102 Composition of jovian dust stream particles. *Icarus*, 183:122–134.
- 1103 Showalter, M. R., de Pater, I., Verbanac, G., Hamilton, D. P., and Burns, J. A. (2008).
1104 Properties and Dynamics of Jupiter’s Gossamer Rings from Galileo, Voyager, Hubble
1105 and Keck Images. *Icarus*, 195:361–377.
- 1106 Spencer, J. R., Stern, S. A., Cheng, A. F., Weaver, H. A., Reuter, D. C., Retherford, K.,
1107 Lunsford, A., Moore, J. M., Abramov, O., Lopes, R. M. C., Perry, J. E., Kamp, L.,
1108 Showalter, M., Jessup, K. L., Marchis, F., Schenk, P. M., and Dumas, C. (2007). Io
1109 Volcanism Seen by New Horizons: A Major Eruption of the Tvashtar Volcano. *Science*,
1110 318:240–243.
- 1111 Sremčević, M., Krivov, A. V., Krüger, H., and Spahn, F. (2005). Impact-generated dust
1112 clouds around planetary satellites: model versus Galileo data. *Planetary and Space
1113 Science*, 53:625–641.
- 1114 Sremčević, M., Krivov, A. V., and Spahn, F. (2003). Impact-generated dust clouds around
1115 planetary satellites: Asymmetry effects. *Planetary and Space Science*, 51:455–471.
- 1116 Svestka, J., Auer, S., Baguhl, M., and Grün, E. (1996). Measurements of dust electric
1117 charges by the Ulysses and Galileo dust detectors. In Gustafson, B. A. and Hanner,
1118 M. S., editors, *Physics, Chemistry and Dynamics of Interplanetary Dust, ASP Confer-
1119 ence Series*, volume 104, pages 481–484.

- 1120 Thiessenhusen, K.-U., Krüger, H., Spahn, F., and Grün, E. (2000). Dust grains around
1121 Jupiter – The observations of the Galileo Dust Detector. *Icarus*, 144:89–98.
- 1122 Willis, M. J., Burchell, M., Ahrens, T. J., Krüger, H., and Grün, E. (2005). Decreased
1123 values of cosmic dust number density estimates in the solar system. *Icarus*, 176:440–
1124 452.
- 1125 Willis, M. J., Burchell, M., Cole, M., and McDonnell, J. A. M. (2004). Influence of impact
1126 ionization detection methods on determination of dust particle flux in space. *Planetary
1127 and Space Science*, 52:711–725.
- 1128 Zook, H. A., Grün, E., Baguhl, M., Hamilton, D. P., Linkert, G., Linkert, D., Liou, J.-C.,
1129 Forsyth, R., and Phillips, J. L. (1996). Solar wind magnetic field bending of Jovian dust
1130 trajectories. *Science*, 274:1501–1503.

Table 1: Summary of Galileo dust data papers and significant mission events.

Time Interval	Significant Mission Events	Paper Number
1989 – 1992	Galileo launch (18 Oct 1989)	II (Grün et al., 1995a)
1993 – 1995	Jupiter orbit insertion (7 Dec 1995)	IV (Krüger et al., 1999a)
1996	Galileo orbits G1 – E4	VI (Krüger et al., 2001a)
1997 – 1999	Galileo orbits J5 – I25	VIII (Krüger et al., 2006b)
2000 – 2003	Galileo orbits E26 – J35, First gossamer ring passage (5 Nov 2002), second gossamer ring passage and Galileo Jupiter impact (21 Sep 2003)	X (this paper)

Table 2: Galileo mission and dust detector (DDS) configuration, tests and other events (2000-2003). See text for details.

Yr-day	Date	Time	Event
89-291	18 Oct 1989	16:52	Galileo launch
95-341	07 Dec 1995	21:54	Galileo Jupiter closest approach, distance: 4.0R _J
99-345	11 Dec 1999	02:07	DDS configuration: HV=4, EVD=I, SSEN=0,1,1,1
00-001	01 Jan 2000	00:00	DDS begin RTS data
00-003	03 Jan 2000	17:28	DDS end RTS data, begin record data
00-003	03 Jan 2000	18:00	Galileo Europa 26 (E26) closest approach , altitude 351 km
00-003	03 Jan 2000	18:30	DDS end record data, begin RTS data
00-004	04 Jan 2000	03:33	Galileo Jupiter closest approach, distance 5.8R _J
00-006	06 Jan 2000	02:00	Galileo turn 5°, duration 3 h, return to nominal attitude
00-007	07 Jan 2000	19:00	Galileo OTM-82, size of turn 3°, duration 5 h, return to nominal attitude
00-009	09 Jan 2000	11:49	DDS end RTS data
00-029	29 Jan 2000	04:00	Galileo OTM-83, size of turn 3°, duration 3 h, return to nominal attitude
00-033	02 Feb 2000	18:00	Galileo turn 4°, new nominal attitude
00-038	07 Feb 2000	23:00	Galileo turn 7°, duration 3 h, return to nominal attitude
00-049	18 Feb 2000	16:36	Galileo OTM-84, no attitude change
00-050	19 Feb 2000	12:00	DDS begin RTS data
00-053	22 Feb 2000	12:30	Galileo Jupiter closest approach, distance 5.9R _J
00-053	22 Feb 2000	13:02	DDS end RTS data, begin record data
00-053	22 Feb 2000	13:47	Galileo Io 27 (I27) closest approach , altitude 198 km
00-053	22 Feb 2000	14:25	DDS end record data, begin RTS data
00-054	23 Feb 2000	19:20	DDS last RTS data before spacecraft anomaly
00-055	24 Feb 2000	04:00	Galileo turn 15°, duration 30 h, return to nominal attitude
00-055	24 Feb 2000	21:00	Galileo spacecraft anomaly
00-056	25 Feb 2000	04:16	DDS begin RTS data after spacecraft anomaly
00-057	25 Feb 2000	14:00	Galileo OTM-85, size of turn 19°, duration 11 h, return to nominal attitude
00-059	28 Feb 2000	23:56	DDS end RTS data
00-070	10 Mar 2000	10:00	Galileo turn 8°, new nominal attitude
00-088	28 Mar 2000	00:00	Galileo turn 3°, duration 3 h, return to nominal attitude
00-098	07 Apr 2000	12:00	Galileo OTM-86, no attitude change
00-116	25 Apr 2000	20:00	Galileo turn 8°, new nominal attitude
00-117	26 Apr 2000	01:11	DDS last MRO before solar conjunction
00-118	27 Apr 2000		Start solar conjunction period
00-138	17 May 2000		End solar conjunction period
00-138	17 May 2000	09:30	DDS begin RTS data
00-139	18 May 2000	10:00	Galileo OTM-87, no attitude change
00-141	20 May 2000	09:39	DDS end RTS data, begin record data
00-141	20 May 2000	10:10	Galileo Ganymede 28 (G28) closest approach , altitude 808 km

Abbreviations used: MRO: DDS memory readout; HV: channeltron high voltage step; EVD: event definition, ion- (I), channeltron- (C), or electron-channel (E); SSEN: detection thresholds, ICP, CCP, ECP and PCP; OTM: orbit trim maneuver; RTS: Realtime science.

Table 2: Continued.

Yr-day	Date	Time	Event
00-141	20 May 2000	10:40	DDS end record data, begin RTS data
00-142	21 May 2000	04:52	Galileo Jupiter closest approach, distance $6.7R_J$
00-143	22 May 2000	08:00	Galileo turn 2° , duration 1 h, return to nominal attitude
00-146	25 May 2000	08:00	Galileo OTM-88, no attitude change
00-152	31 May 2000	07:00	Galileo turn 8° , new nominal attitude
00-170	18 Jun 2000	23:57	DDS end RTS data
00-176	23 Jun 2000	03:00	Galileo turn 7° , duration 2 h, return to nominal attitude
00-189	07 Jul 2000	19:00	Galileo turn 9° , new nominal attitude
00-209	27 Jul 2000	11:11	DDS configuration: HV = 5
00-216	03 Aug 2000	18:31	DDS begin RTS data
00-223	10 Aug 2000	02:00	Galileo turn 9° , new nominal attitude
00-244	31 Aug 2000	16:00	Galileo turn 2° , duration 2 h, return to nominal attitude
00-252	08 Sep 2000	18:00	Galileo OTM-89, size of turn 2° , duration 3 h, return to nominal attitude
00-253	09 Sep 2000	08:11	DDS end RTS data
00-300	26 Oct 2000	10:01	DDS begin RTS data
00-302	28 Oct 2000	01:00	Galileo OTM-90, no attitude change
00-342	07 Dec 2000	23:00	Galileo turn 2° , duration 1 h, return to nominal attitude
00-353	18 Dec 2000	05:00	Galileo turn 20° , new nominal attitude
00-356	21 Dec 2000	20:15	Galileo OTM-91, no attitude change
00-363	28 Dec 2000	08:25	Galileo Ganymede 29 (G29) closest approach , altitude 2,337 km
00-364	29 Dec 2000	03:27	Galileo Jupiter closest approach, distance $7.5R_J$
01-002	02 Jan 2001	20:00	Galileo OTM-92, no attitude change
01-004	04 Jan 2001	03:30	Galileo turn 10° , return to nominal attitude
01-086	27 Mar 2001	23:00	DDS end RTS data
01-094	04 Apr 2001	04:00	Galileo turn 8° , new nominal attitude
01-114	24 Apr 2001	03:00	Galileo turn 8° , duration 9 h, return to nominal attitude
01-130	10 May 2001	16:00	Galileo OTM-94, no attitude change
01-133	13 May 2001	01:00	Galileo turn 4° , new nominal attitude
01-142	22 May 2001	23:00	Galileo turn 6° , return to nominal attitude
01-143	23 May 2001	12:01	DDS begin RTS data
01-143	23 May 2001	17:33	Galileo Jupiter closest approach, distance $7.3R_J$
01-145	25 May 2001	11:24	Galileo Callisto 30 (C30) closest approach , altitude 138 km
01-146	26 May 2001	07:15	DDS end RTS data
01-146	26 May 2001	09:00	Galileo turn 5° , duration 2 h, return to nominal attitude
01-146	26 May 2001	22:00	Galileo turn 12° , duration 13 h, return to nominal attitude
01-148	28 May 2001	19:00	Galileo OTM-95, size of turn 1°
01-152	01 Jun 2001	11:00	Galileo turn 5° , new nominal attitude
01-154	03 Jun 2001	16:58	DDS last MRO before solar conjunction
01-155	04 Jun 2001		Start solar conjunction period
01-174	23 Jun 2001		End solar conjunction period

Table 2: Continued.

Yr-day	Date	Time	Event
01-177	26 Jun 2001	22:58	DDS fist MRO after solar conjunction
01-183	02 Jul 2001	21:00	Galileo turn 4°, new nominal attitude
01-186	05 Jul 2001	05:00	Galileo turn 5°, duration 5 h, return to nominal attitude
01-194	13 Jul 2001	06:00	Galileo OTM-97, size of turn 3°, duration 4 h, return to nominal attitude
01-201	20 Jul 2001	07:00	Galileo turn 4°, new nominal attitude
01-215	03 Aug 2001	23:00	Galileo OTM-98, no attitude change
01-217	05 Aug 2001	05:12	DDS begin RTS data
01-218	06 Aug 2001	04:52	Galileo Jupiter closest approach, distance 5.9R _J
01-218	06 Aug 2001	04:59	Galileo Io 31 (I31) closest approach , altitude 193 km
01-219	07 Aug 2001	16:08	DDS end RTS data
01-220	08 Aug 2001	03:00	Galileo turn 7°, duration 2 h, return to nominal attitude
01-222	10 Aug 2001	19:30	Galileo OTM-99, no attitude change
01-224	12 Aug 2001	08:00	Galileo turn 3°, new nominal attitude
01-236	24 Aug 2001	07:00	Galileo turn 3°, duration 2 h, return to nominal attitude
01-245	02 Sep 2001	03:00	Galileo OTM-100, no attitude change
01-246	03 Sep 2001	05:00	Galileo turn 4°, new nominal attitude
01-261	18 Sep 2001	12:00	Galileo OTM-101, no attitude change
01-270	27 Sep 2001	04:00	Galileo turn 3°, new nominal attitude
01-286	13 Oct 2001	18:00	Galileo OTM-102, no attitude change
01-287	14 Oct 2001	02:04	DDS begin RTS data
01-288	15 Oct 2001	23:56	Galileo Jupiter closest approach, distance 5.8R _J
01-289	16 Oct 2001	01:23	Galileo Io 32 (I32) closest approach , altitude 184 km
01-290	17 Oct 2001	12:00	Galileo turn 3°, duration 2 h, return to nominal attitude
01-293	20 Oct 2001	04:00	Galileo OTM-103, size of turn 1°, duration 2 h, return to nominal attitude
01-301	28 Oct 2001	23:30	DDS end RTS data
01-324	20 Nov 2001	00:00	Galileo turn 4°, duration 2 h, return to nominal attitude
01-335	01 Dec 2001	00:00	Galileo OTM-104, no attitude change
01-340	06 Dec 2001	15:00	Galileo turn 2°, new nominal attitude
01-352	18 Dec 2001	00:00	DDS configuration: HV = 6
01-357	23 Dec 2001	16:00	Galileo turn 2°, new nominal attitude
02-004	04 Jan 2002	12:25	DDS begin RTS data
02-010	10 Jan 2002	00:00	Galileo turn 5°, duration 2 h, new nominal attitude
02-017	17 Jan 2002	09:15	DDS end RTS data
02-017	17 Jan 2002	13:40	Galileo spacecraft anomaly
02-017	17 Jan 2002	14:08	Galileo Io 33 (I33) closest approach , altitude 102 km
02-017	17 Jan 2002	16:23	Galileo Jupiter closest approach, distance 5.5R _J
02-017	17 Jan 2002	23:50	DDS begin RTS data after spacecraft anomaly
02-021	21 Jan 2002	12:00	Galileo OTM-106, no attitude change
02-029	29 Jan 2002	23:00	Galileo turn 2°, new nominal attitude
02-032	01 Feb 2002	01:00	Galileo turn 44°, duration 90 h, return to nominal attitude
02-047	16 Feb 2002	19:09	Galileo spacecraft anomaly
02-051	20 Feb 2002	17:54	DDS begin RTS data after spacecraft anomaly
02-094	04 Apr 2002	00:00	Galileo turn 3°, duration 3 h, return to nominal attitude

Table 2: Continued.

Yr-day	Date	Time	Event
02-102	12 Apr 2002	05:00	Galileo turn 3°, new nominal attitude
02-124	04 May 2002	23:00	Galileo turn 4°, new nominal attitude
02-131	11 May 2002	12:00	Galileo turn 1°, duration 2 h, return to nominal attitude
02-146	26 May 2002	02:00	Galileo turn 4°, new nominal attitude
02-157	06 Jun 2002	02:00	Galileo turn 6°, duration 3 h, return to nominal attitude
02-165	14 Jun 2002	16:00	Galileo OTM-107, size of turn 3°, duration 3 h, return to nominal attitude
02-182	01 Jul 2002	11:00	Galileo turn 12°, new nominal attitude
02-190	09 Jul 2002		Begin solar conjunction
02-209	28 Jul 2002		End solar conjunction
02-214	02 Aug 2002	08:00	Galileo turn 5°, new nominal attitude
02-232	20 Aug 2002	15:00	Galileo turn 4°, new nominal attitude
02-250	07 Sep 2002	12:00	Galileo turn 4°, new nominal attitude
02-274	01 Oct 2002	19:30	Galileo spacecraft anomaly
02-275	02 Oct 2002	23:54	DDS begin RTS after spacecraft anomaly
02-281	08 Oct 2002	02:00	Galileo turn 6°, duration 3 h, return to nominal attitude
02-285	12 Oct 2002	15:00	Galileo turn 9°, new nominal attitude
02-298	25 Oct 2002	03:00	Galileo turn 2°, duration 2 h, return to nominal attitude
02-309	05 Nov 2002	02:44	DDS end RTS data
02-309	05 Nov 2002	02:44	DDS begin record data
02-309	05 Nov 2002	06:19	Galileo Amalthea 34 (A34) closest approach , 244 km distance from moon's centre
02-309	05 Nov 2002	06:35	Galileo spacecraft anomaly, end record data
02-309	05 Nov 2002	07:25	Galileo Jupiter closest approach, distance 2.0R _J
02-318	14 Nov 2002	08:00	Galileo turn 9°, duration 3 h, return to nominal attitude
02-322	18 Nov 2002	14:29	DDS first MRO after spacecraft anomaly
02-363	29 Dec 2002	07:53	DDS final MRO
03-003	03 Jan 2003	22:00	Galileo turn 20°, duration 6 h, return to nominal attitude
03-004	04 Jan 2003	21:00	Galileo turn 20°, duration 5 h, return to nominal attitude
03-008	08 Jan 2003	08:00	Galileo turn 17°, duration 2 h, return to nominal attitude
03-010	10 Jan 2003	22:00	Galileo turn 22°, duration 82 h, return to nominal attitude
03-015	15 Jan 2003	10:00	Galileo turn 22°, new nominal attitude
03-063	04 Mar 2003	15:00	DDS begin RTS data
03-070	11 Mar 2003	21:50	DDS end RTS data
03-255	12 Sep 2003	21:43	DDS begin RTS data
03-256	13 Sep 2003	18:57	DDS end RTS data
03-263	20 Sep 2003	13:44	DDS begin RTS data
03-263	20 Sep 2003	14:26	DDS end RTS data
03-264	21 Sep 2003	12:10	DDS begin RTS data
03-264	21 Sep 2003	17:59	DDS end RTS data
03-264	21 Sep 2003	18:57	Galileo Jupiter impact, end of mission

Table 3: Dust detector sensitive area and field-of-view (FOV) for different dust data sets.

Dust data set	FOV (°)	Sensor area (cm ²)	Comment
Stream particles class 2	140	1000	Nominal target FOV (Grün et al., 1992a)
Stream particles class 3	96	110	Reduced target FOV (Krüger et al., 1999b)
All other	180	1000	Target plus side wall FOV (Altobelli et al., 2004)

Table 4: Details of Galileo dust data transmission modes during the Jupiter mission. See text for details.

	Realtime Science (RTS)		Record	MROs	
	Low rate	High rate			
Data rate (bits s ⁻¹)	1.1	3.4	24	$\sim 3 \times 10^{-3}{}^a)$	
Timing accuracy (min)	21.2	7.1	~ 1	259	
Data frames per readout		7	7	46	
Mission time coverage (%)		40	< 0.1	60	
Maximum event rate recordable by accumulators (min ⁻¹)	AC21/AC31 ^{b)}	3000	9000	65000	$\approx 2^a)$
	All other	12	36	256	$\approx 0.01^a)$
Maximum event rate for full data set transmission (min ⁻¹)		$\frac{1}{21.2}$	$\frac{1}{7.1}$	~ 1	$\approx \frac{46}{20\text{days}}$

^{a)} One MRO every 20 days assumed.

^{b)} Since 4 December 1996; the “All other” row was valid for all data before this time.

Table 5: Criteria for the separation of noise events in classes 1 and 2 from true dust impacts in the region within Io’s orbit for Galileo orbits A34 and J35 (gossamer ring passages). Noise events in the lowest amplitude range (AR1) fulfill at least one of the criteria listed, whereas noise events in the higher ranges fulfill two criteria (from Moissl, 2005).

Class, AR	EA - IA		CA	EIC
Class 1, AR1	≤ 2 or ≥ 9	or	≤ 2	–
Class 1, AR2-6	≤ 2 or ≥ 9	and	≤ 2	–
Class 2, AR1	–		–	= 0
Class 2, AR2-6	≤ 1 or ≥ 7	and	≤ 2	–

Table 6: Overview of dust impacts accumulated with Galileo DDS between 1 January 2000 and 21 September 2003. The jovicentric distance D_{JUP} , the length of the time interval Δt (days) from the previous table entry, and the corresponding numbers of impacts are given for the class 2 and 3 accumulators. The accumulators are arranged with increasing signal amplitude ranges (AR), e.g. AC31 means counter for CLN = 3 and AR = 1. The determination of the noise contamination f_{noi} in class 2 is described in Paper VI. The Δt in the first line (day 00-002) is the time interval counted from the last entry in Table 2 in Paper VIII. The totals of counted impacts, of impacts with complete data, and of all events (noise plus impact events) for the entire period are given as well.

Date	Time	D_{JUP} [R _J]	Δt [d]	$f_{noi,AC21}$	AC 21*	AC 31*	$f_{noi,AC22}$	AC 22	AC 32	$f_{noi,AC23}$	AC 23	AC 33	$f_{noi,AC24}$	AC 24	AC 34
00-002	23:46	19.28	21.06	0.81	8	-	0.00	-	-	-	-	-	-	-	-
00-003	21:55	7.570	0.922	0.27	521	40	0.50	1	1	0.00	1	2	-	-	-
00-005	10:08	20.06	1.908	0.54	552	9	0.00	2	1	-	-	-	0.00	1	1
00-032	13:39	13.96	0.791	0.57	301	8	0.00	4	1	-	-	-	-	-	-
00-053	10:26	6.120	0.796	0.56	301	8	0.00	4	1	-	-	-	-	-	-
00-056	22:40	42.65	3.510	0.80	869	-	0.80	20	2	0.00	1	-	0.00	3	2
00-074	20:37	126.1	17.91	0.59	17	-	0.50	2	1	-	-	-	-	-	-
00-141	14:34	12.54	66.74	0.96	20	2	0.25	4	-	-	-	-	-	-	-
00-143	23:11	27.10	2.359	0.50	209	-	0.00	2	-	-	-	-	-	-	-
00-149	19:41	76.24	5.853	0.10	89	3	-	-	-	-	-	-	-	-	-
00-177	07:37	193.7	27.49	0.23	42	3	0.50	2	-	-	-	-	-	-	-
00-206	19:08	256.7	29.47	0.72	5383	160	-	-	-	-	-	1	-	-	-
00-216	23:50	270.0	10.19	0.00	4422	115	-	-	-	-	-	-	-	-	-
00-220	17:43	3.745	0.00	13922	522	222	1.00	1	-	-	-	-	-	-	-
00-222	23:09	276.2	2.226	0.00	3964	219	-	-	-	-	-	-	-	-	-
00-228	05:08	280.6	5.249	0.00	2648	203	-	-	-	-	-	-	-	-	-
00-231	18:47	283.1	3.568	0.00	5590	424	-	-	-	-	-	-	-	-	-
00-236	10:15	285.7	4.644	0.00	10750	842	-	-	-	-	-	-	-	-	-
00-246	03:28	289.1	9.717	0.00	33125	3489	0.00	2	-	-	-	-	-	-	-
00-256	11:57	289.6	10.35	0.01	49616	3149	0.00	1	-	-	-	-	-	-	-
00-266	13:29	287.1	10.06	0.00	47774	2768	-	-	1	-	-	-	-	-	-
00-276	00:28	281.8	9.457	0.00	17821	5196	-	-	-	-	-	-	-	-	-
00-300	11:26	254.7	24.45	0.00	3200	163	-	-	-	-	-	-	-	-	-
00-306	12:10	244.7	6.030	0.01	161	3	-	-	-	-	-	-	-	-	-
00-326	08:51	200.4	19.86	0.05	223	9	-	-	-	-	-	-	-	-	-
00-363	16:33	10.84	37.32	0.37	68	1	0.00	1	1	-	-	-	-	-	-
00-366	00:38	27.82	2.532	0.18	1014	41	0.00	3	-	-	-	-	-	-	-
00-366	23:49	37.39	0.973	0.04	345	19	-	-	-	0.00	1	-	-	-	-
01-002	14:24	51.27	6.607	0.09	513	47	-	-	-	-	-	-	-	-	-
01-006	08:59	77.49	3.774	0.00	661	47	-	-	-	-	-	-	-	-	-
01-010	13:29	100.5	4.187	0.05	312	15	-	-	-	-	-	-	-	-	-
01-015	02:55	122.8	4.969	0.07	373	24	-	-	-	-	-	-	-	-	-
01-040	14:08	14.86	14.86	0.06	365	4	-	-	-	-	-	-	-	-	-
01-096	14:04	198.7	55.70	0.11	59	3	0.33	3	-	-	-	-	-	-	-

Table 6 continued.

Date	Time	D_{imp} [K]	Δt [d]	$f_{noi,AC21}$	AC 21*	AC 31*	$f_{noi,AC22}$	AC 22	AC 32	$f_{noi,AC23}$	AC 23	AC 33	$f_{noi,AC24}$	AC 24	AC 34
01-143	15:55	7.390	47.07	0.40	3245	45	0.44	9	2	-	-	-	-	-	-
01-146	06:32	34.34	2.609	0.60	2913	129	0.18	11	1	-	-	-	0.00	2	-
01-154	16:58	8.712	8.434	0.18	16888	756	0.00	1	1	-	-	-	-	-	-
01-177	20:07	136.1	23.13	0.00	38739	1940	0.00	1	-	-	-	-	-	-	-
01-194	13:03	124.8	16.70	0.00	4139	586	-	-	-	-	-	-	-	-	-
01-209	11:19	76.61	14.92	0.01	394	31	0.00	1	1	0.00	1	1	0.33	3	2
01-218	07:24	6.280	8.836	0.47	351	6	0.00	5	4	-	-	-	0.00	2	-
01-221	21:01	44.16	3.567	0.45	207	8	0.33	6	-	-	-	-	0.00	-	-
01-246	07:41	128.5	24.44	0.01	509	9	0.00	1	-	-	-	-	-	-	-
01-288	01:25	16.92	41.73	0.06	243	14	-	-	-	-	-	-	-	-	-
01-291	11:32	34.37	3.420	0.73	303	1	0.00	2	2	0.00	2	-	0.50	2	-
01-314	06:33	137.8	22.78	0.33	51	-	-	-	-	-	-	-	-	-	-
01-348	23:00	152.6	34.69	0.33	19	1	0.00	2	-	-	-	-	-	-	-
02-017	02:52	12.09	33.16	0.57	36	-	0.00	1	1	-	-	-	0.00	2	1
02-018	00:32	8.820	0.902	0.86	341	-	0.00	1	2	-	-	-	0.00	2	2
02-032	03:41	118.4	14.13	0.51	80	3	0.20	5	2	0.00	1	-	-	-	-
02-069	12:20	247.7	37.36	0.30	47	1	-	-	-	-	-	-	-	-	-
02-106	03:02	312.8	36.61	0.48	23	-	-	-	-	-	-	-	-	-	-
02-151	13:43	346.5	45.44	0.17	29	1	0.00	1	-	-	-	-	-	-	-
02-184	10:32	343.9	32.86	0.27	22	-	-	-	-	-	-	-	-	-	-
02-222	06:37	312.7	37.83	0.88	24	1	-	-	-	-	-	-	-	-	-
02-262	21:04	238.9	43.66	0.81	19	3	-	-	-	-	-	-	-	-	-
02-306	10:19	42.73	40.55	0.06	18	-	0.00	1	1	-	-	-	-	-	-
02-308	21:03	11.18	2.447	0.52	55	3	-	-	2	0.00	3	1	-	-	2
02-309	04:21	4.540	0.304	0.80	17	-	0.00	2	2	-	-	-	-	-	-
02-309	05:32	3.320	0.048	0.83	77	-	-	-	-	0.00	2	-	-	-	-
02-329	16:36	171.7	14.43	0.63	57	5	0.14	21	1	0.00	2	1	0.00	15	5
02-357	20:16	245.2	34.15	0.04	92	80	0.00	191	2	0.00	46	1	0.00	62	1
03-066	18:08	557.0	73.91	0.86	11	1	-	-	-	-	-	-	-	-	2
03-262	11:23	38.06	195.7	0.00	28	1	0.00	2	5	0.00	1	-	-	-	1
03-264	14:11	7.190	2.117	0.00	36	1	0.00	14	1	0.00	1	1	0.00	1	1
03-264	15:48	5.200	0.063	0.53	41	-	-	-	-	0.00	1	2	-	-	-
03-264	17:39	2.340	0.094	0.53	124	-	0.00	45	8	0.42	26	10	0.12	68	36
Events (counted)				-	284545	20976	-	372	45	-	107	23	-	163	59
Impacts (complete data)				-	3291	1865	-	68	38	-	36	16	-	26	28
All events(complete data)				0.22	4229	1865	0.28	95	41	0.05	38	16	0.07	28	28

*: AC21 and AC31: Overflows of the 8 bit accumulators were counted with overflow counters so that no unrecognized overflows occurred in these two channels.
 f_{noi} has been estimated from the data sets transmitted.

No.	IMP.DATE	TEV	C	AR	S	IA	EA	CA	IT	ET	E	E	I	E	I	PA	P	E	E	I	E	C	C	P	C	P	HV	LON	LAT	D _{dup}	ROT	S _{LON}	S _{LAT}	V	VEF	M	MEF
21240	03-264 17:36:50	8	3	2	166	14	26	5	15	15	14	0	1	1	25	1	5	0	1	1	1	1	1	1	1	6	150.5	1.0	3.066	217	117	-38	2.0	1.9	2.2-10-09	10.5	
21241	03-264 17:43:55	8	3	4	241	24	12	12	14	6	6	0	1	1	49	1	5	0	1	1	1	1	1	1	6	150.5	1.0	2.894	111	208	-14	2.0	1.9	1.2-10-09	10.5		
21242	03-264 17:43:55	8	2	2	246	12	22	5	15	14	15	0	1	1	18	5	5	0	1	1	1	1	1	1	6	150.5	1.0	2.894	104	209	-8	2.0	1.9	8.0-10-10	10.5		
21243	03-264 17:50:59	8	3	4	186	30	56	25	14	14	7	0	1	1	26	1	5	0	1	1	1	1	1	1	6	150.5	1.0	2.720	188	144	-50	2.0	1.9	2.0-10-07	10.5		
21244	03-264 17:50:59	8	3	2	33	14	24	8	14	12	13	0	1	1	13	10	5	0	1	1	1	1	1	1	6	150.5	1.0	2.720	44	202	39	2.0	1.9	1.6-10-09	10.5		
21246	03-264 17:59:01	22	3	2	239	9	22	5	14	12	13	0	1	1	37	8	5	0	1	1	1	1	1	1	6	150.5	1.0	2.518	114	207	-16	2.0	1.9	4.9-10-10	10.5		
21248	03-264 17:59:01	22	3	4	4	24	28	25	15	10	5	0	1	1	46	14	5	0	1	1	1	1	1	1	6	150.5	1.0	2.518	84	210	7	4.9	2.1	4.6-10-10	14.3		
21249	03-264 17:59:01	22	3	3	44	21	22	5	13	14	8	0	1	1	49	6	5	0	1	1	1	1	1	1	6	150.5	1.0	2.518	28	191	49	2.0	1.9	2.4-10-09	10.5		
21250	03-264 17:59:01	22	3	4	172	27	11	18	9	3	10	0	1	1	27	2	5	0	1	1	1	1	1	1	6	150.5	1.0	2.518	208	123	-42	7.2	1.9	1.9-10-11	10.5		

Table 6: Slopes α of power law fits to the measured dust flux profiles and Io's dust production.

Orbit	Distance (R_J)	Time interval	α	Dust Production (kg s^{-1})
G1	48 – 15	96-175 to 96-179	-1.9	0.1 – 2
G2	128 – 20	96-214 to 96-250	-4.3	0.2 – 5
C3	113 – 20	96-284 to 96-310	-1.9	0.2 – 10
E4	49 – 20	96-349 to 96-352	-0.7	3 – 20
E6	38 – 15	97-048 to 97-051	-1.6	0.01 – 0.07
G7	59 – 20	97-087 to 97-093	-3.5	0.1 – 5
G8	48 – 20	97-123 to 97-127	-5.4	0.2 – 3
C9	50 – 20	97-173 to 97-177	-2.0	0.07 – 1
C10	55 – 20	97-256 to 97-260	-1.7	0.1 – 5
E11	57 – 20	97-304 to 97-309	-3.7	0.1 – 1
E12	50 – 20	97-344 to 97-348	-2.1	0.05 – 0.7
E14	48 – 20	98-083 to 98-087	-6.1	0.05 – 0.3
E16	39 – 20	98-198 to 98-200	-7.3	0.01 – 0.5
E17	44 – 20	98-265 to 98-268	-1.4	0.05 – 0.5
E18	47 – 33	98-321 to 98-323	-5.6	0.05 – 0.5
E19	48 – 20	99-027 to 99-030	-0.6	0.05 – 0.5
E26	15 – 30	00-005 to 00-006	-5.3	0.01 – 0.05
G28	22 – 167	00-143 to 00-168	-1.8	0.1 – 3
G28	270 – 290	00-227 to 00-252	–	10 – 1000
G29	290 – 172	00-253 to 00-335	+10.4	0.1 – 500
G29	20 – 216	01-365 to 01-070	-2.1	0.01 – 1
I32	22 – 93	01-290 to 01-300	+0.2	0.005 – 0.5
I33	61 – 348	02-023 to 02-164	-1.1	0.05 – 5
A34	348 – 22	02-164 to 02-308	-0.4	0.05 – 1

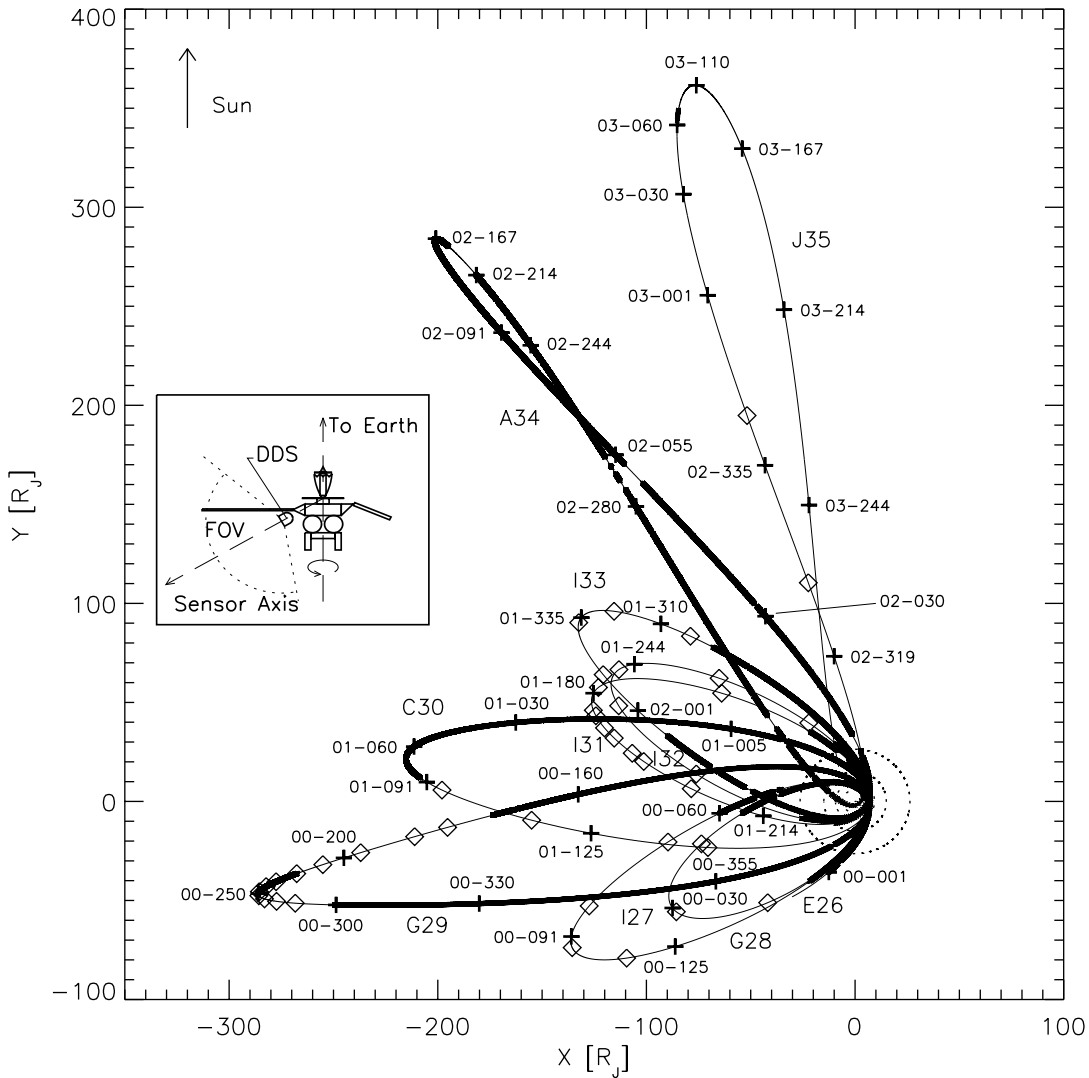


Figure 1: Galileo's trajectory in the jovian system from 2000 to 2003 in a Jupiter-centric coordinate system (thin solid line). Crosses mark the spacecraft position at approximately 30 day intervals (days of year are indicated). Periods when RTS data were obtained are shown as thick solid lines, MROs are marked by diamonds. Galileo's orbits are labelled 'E26', 'I27', 'G28', 'G29', 'C30', 'I31', 'I32', 'I33', 'A34' and 'J35'. Sun direction is to the top and the Sun and Earth directions coincide to within 10° . The orbits of the Galilean moons are indicated (dotted lines). The sketch of the Galileo spacecraft shows the dust detector (DDS), its geometry of dust detection and its field-of-view (FOV). The spacecraft antenna usually pointed towards Earth and the spacecraft made about 3 revolutions per minute.

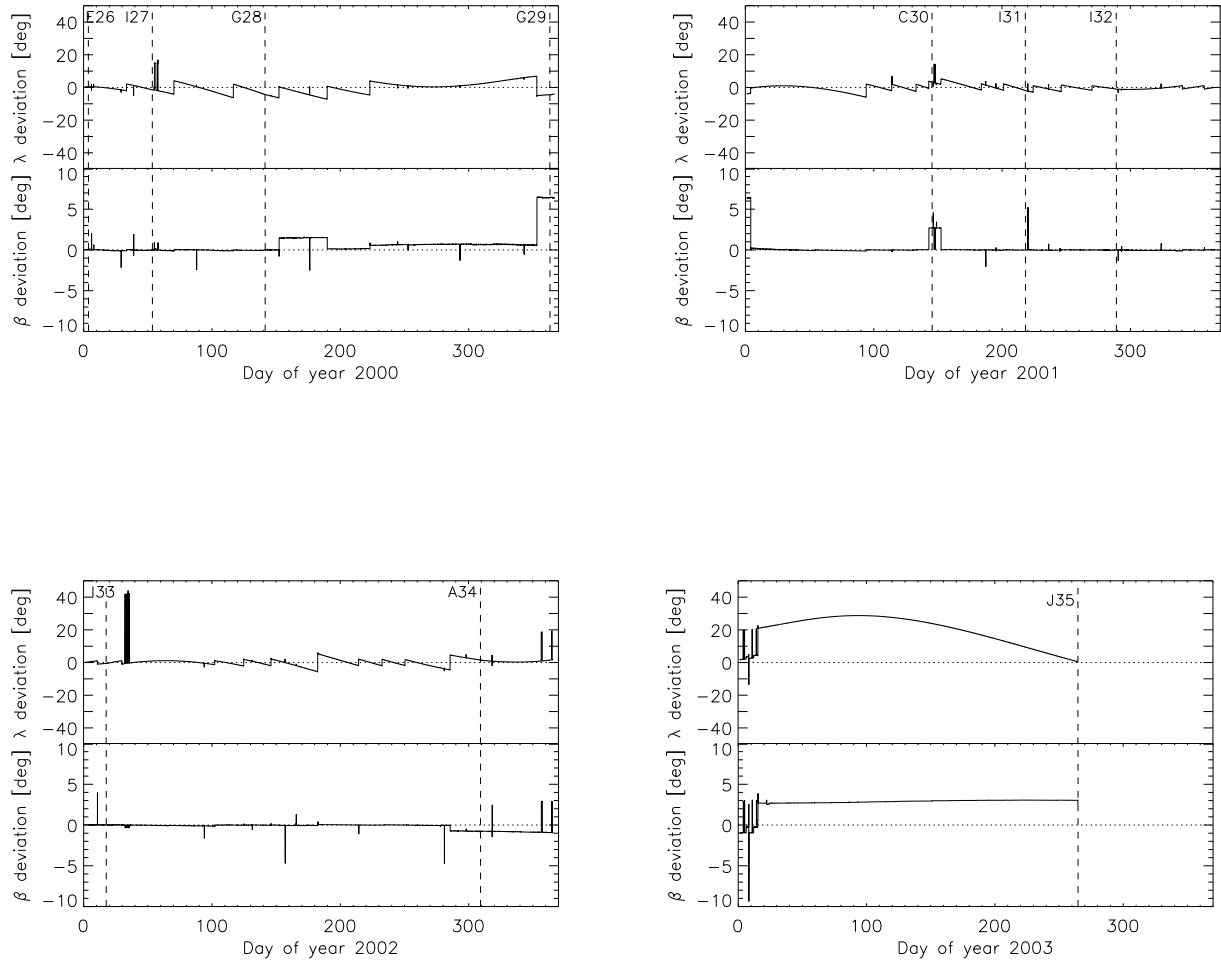


Figure 2: Spacecraft attitude: deviation of the antenna pointing direction (i. e. negative spin axis) from the Earth direction. The angles are given in ecliptic longitude (λ) and latitude (β , equinox 1950.0). Dashed vertical lines indicate satellite flybys (E26-A34) or Galileo’s Jupiter impact (J35). Sharp spikes are associated with imaging observations with Galileo’s cameras or orbit trim maneuvers with the spacecraft thrusters.

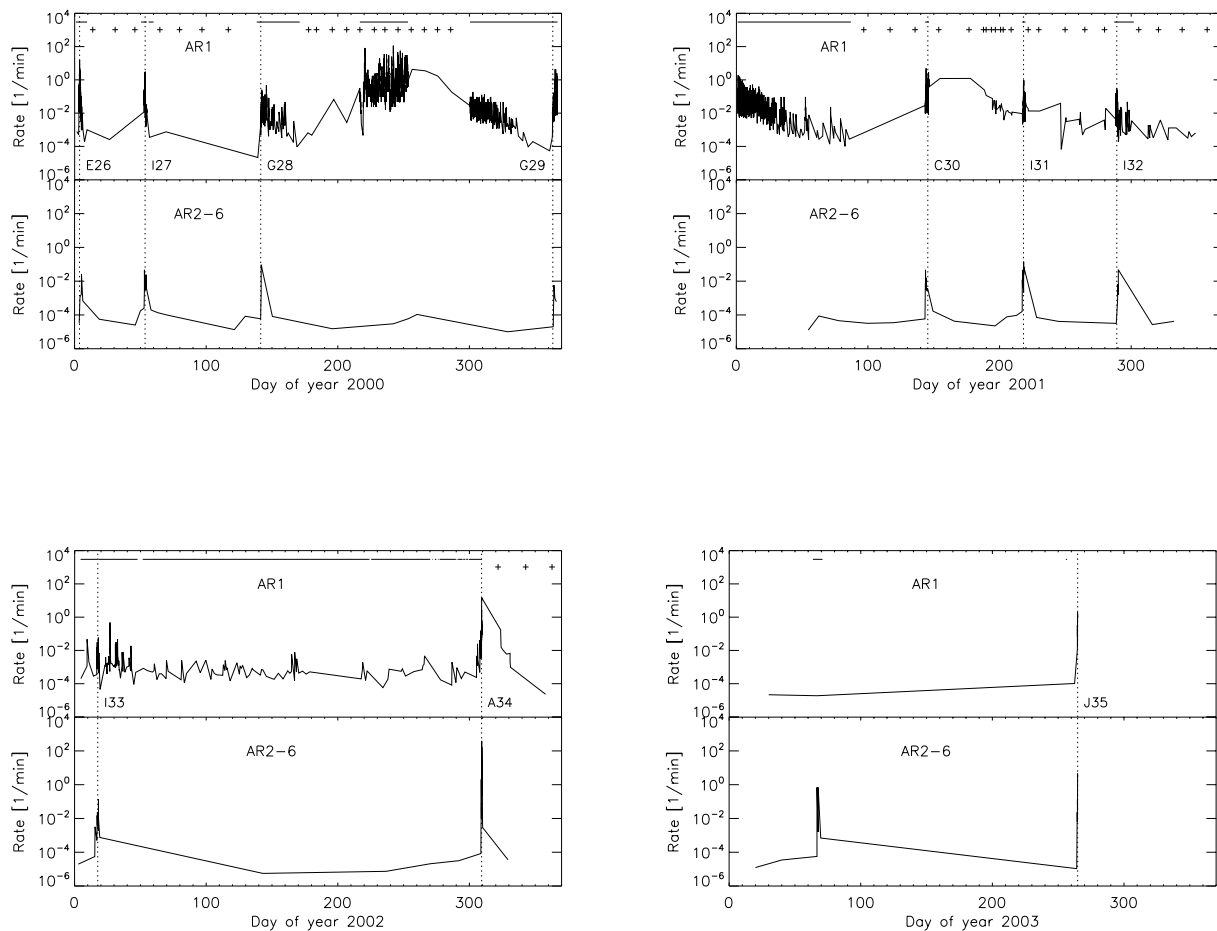


Figure 3: Dust impact rate detected in 2000-2003. For each year the top panel shows the impact rate in AR1 and the bottom panel that for the higher amplitude ranges AR2-6. Only data for classes 2 and 3 are shown. Dotted lines indicate satellite flybys (E26-A34) or Galileo’s Jupiter impact (J35). Perijove passages occurred within two days of the moon closest approaches. These curves are plotted from the number of impacts with the highest time resolution which is available only in electronic form. No smoothing was applied to the data. In the top panels (AR1), time intervals with continuous RTS coverage are indicated by horizontal bars, memory readouts (MROs) are marked by crosses.

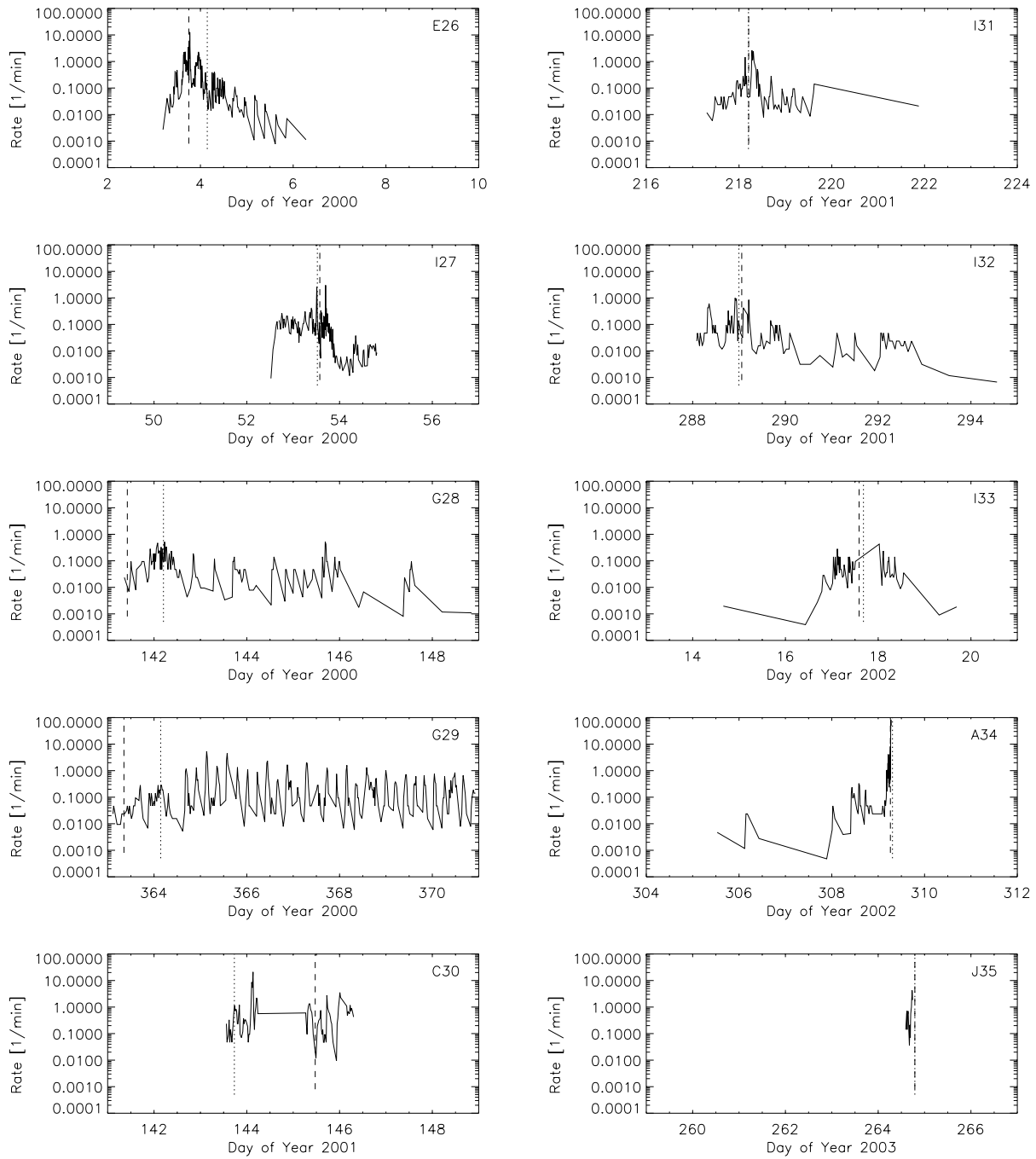


Figure 4: Dust impact rate detected in the inner jovian system in higher time resolution. An 8-day interval is shown in each panel. Only data for AR1 (classes 2 and 3) are shown. Dotted lines indicate perijove passages of Galileo, dashed lines satellite closest approaches (E26-A34) or Jupiter impact (J35).

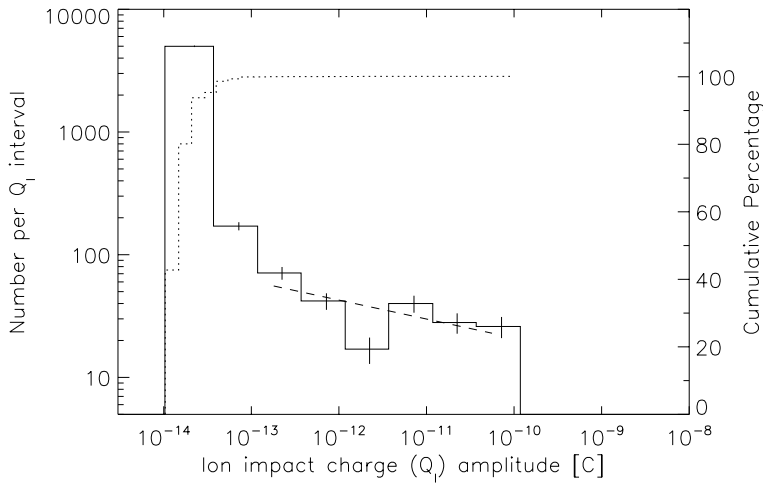


Figure 5: Amplitude distribution of the impact charge Q_I for the 5389 dust particles detected in 2000-2003. The solid line indicates the number of impacts per charge interval, whereas the dotted line shows the cumulative distribution. Vertical bars indicate the \sqrt{n} statistical fluctuation. A power law fit to the data with $Q_I > 10^{-13}$ C (big particles, AR2-4) is shown as a dashed line (Number $N \sim Q_I^{-0.15}$).

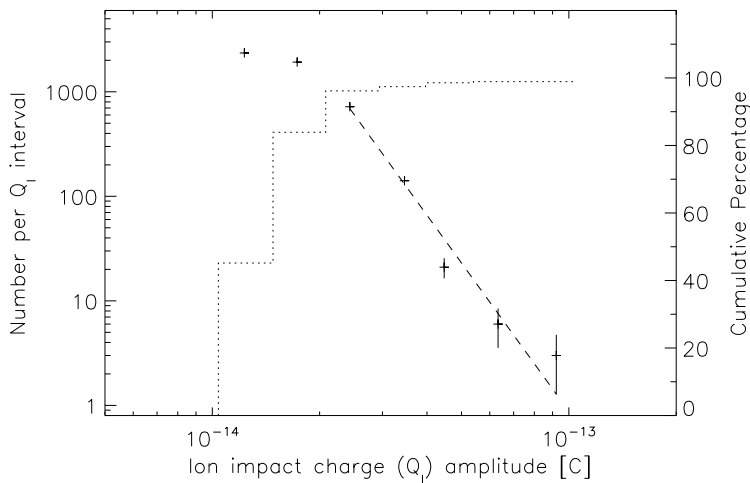


Figure 6: Same as Figure 5 but for the 5165 small particles in the lowest amplitude range (AR1) only. A power law fit to the data with 2×10^{-14} C $< Q_I < 10^{-13}$ C is shown as a dashed line (Number $N \sim Q_I^{-4.72}$).

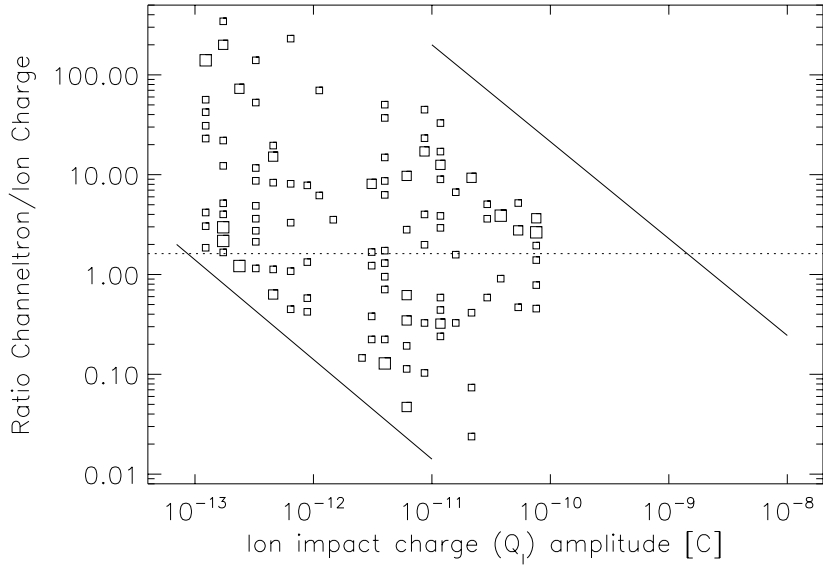


Figure 7: Channeltron amplification factor $A = Q_C/Q_I$ as a function of impact charge Q_I for big particles (AR2-6) detected in 2000-2003. Only impacts measured with a channeltron high voltage setting $HV = 6$ are shown. The solid lines indicate the sensitivity threshold (lower left) and the saturation limit (upper right) of the channeltron. Squares indicate dust particle impacts, and the area of the squares is proportional to the number of events (the scaling of the squares is the same as in Papers VI and VIII). The dotted horizontal line shows the mean value of the channeltron amplification $A = 1.62$ calculated from 65 impacts in the ion impact charge range $10^{-12} \text{ C} < Q_I < 10^{-10} \text{ C}$.

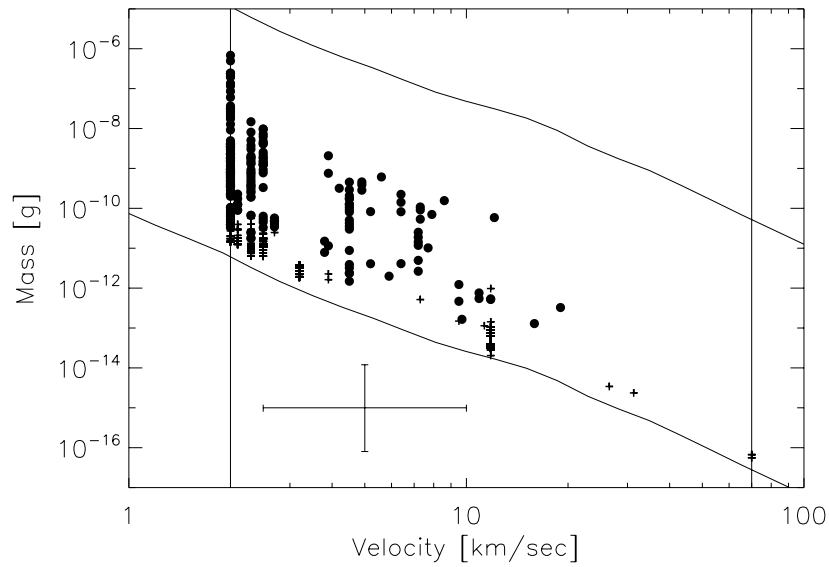


Figure 8: Masses and impact speeds of all 5389 impacts recorded in 2000-2003. The lower and upper solid lines indicate the threshold and saturation limits of the detector, respectively, and the vertical lines indicate the calibrated velocity range. A sample error bar is shown that indicates a factor of 2 error for the velocity and a factor of 10 for the mass determination. Note that all particles are most likely much faster and smaller than implied by this diagram (see text for details). Plus signs show particles in AR1 while filled circles refer to particles in AR2-4. No impacts were measured in AR5 or AR6.

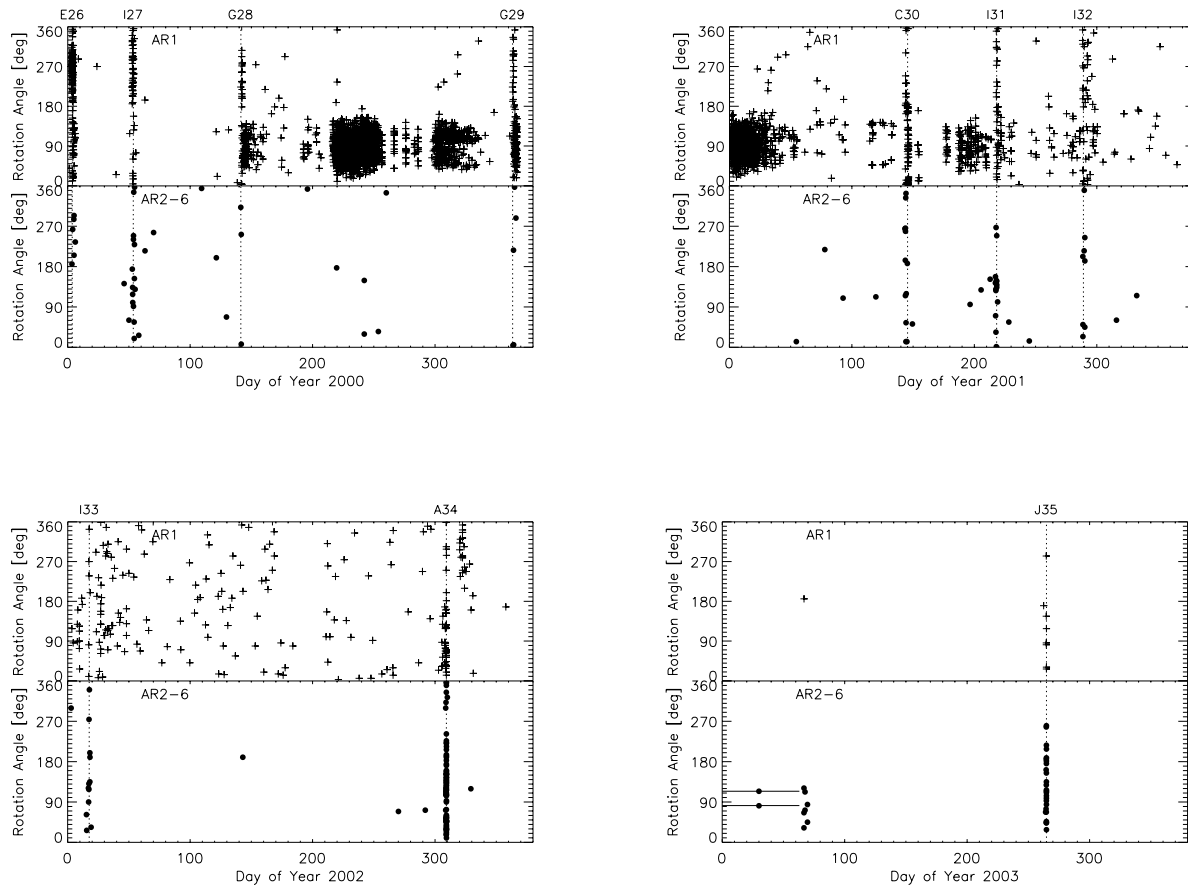


Figure 9: Rotation angle vs. time for two different mass ranges. Upper panel: small particles, AR1; lower panel: big particles, AR2-4. See Section 2 for an explanation of the rotation angle. Vertical dotted lines indicate Galileo’s satellite encounters (E26-A34) or the spacecraft impact into Jupiter (J35). No impacts were measured in AR5 or AR6. The uncertainty in the determination of the impact time is usually much smaller than the symbol sizes, except for two impacts in 2003 which have a very large uncertainty (indicated by two horizontal bars).

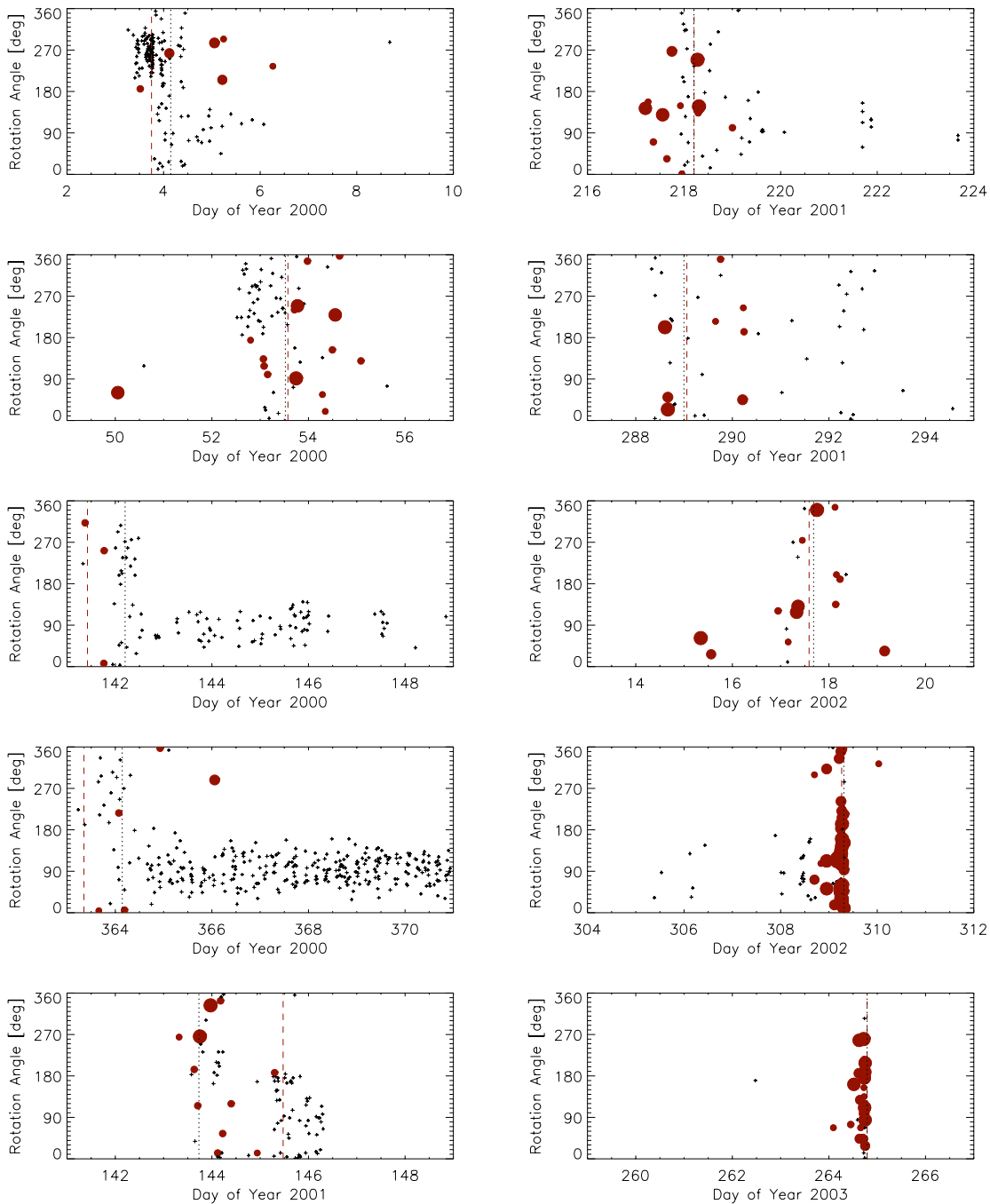


Figure 10: Rotation angle detected by the dust instrument in the inner jovian system in higher time resolution. Only dust data for classes 2 and 3 are shown. Crosses denote impacts in AR1, filled circles those in AR2-4, with the circle size indicating the amplitude range. Dotted lines indicate perijove passages of Galileo, dashed lines satellite closest approaches (E26-A34) or Jupiter impact (J35).

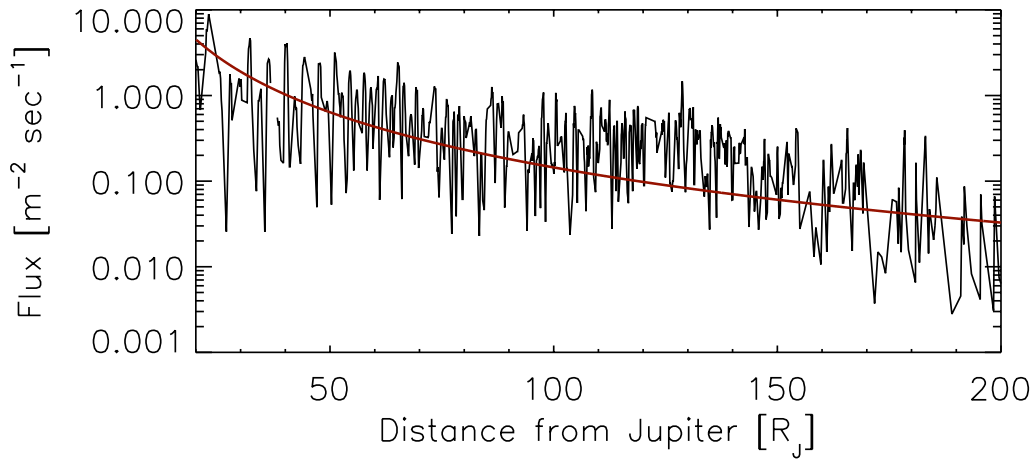


Figure 11: Dust flux measured during Galileo's G29 orbit. The data were smoothed with a 2-hour boxcar average. A power law fit with slope -2.14 is shown. See text for details.

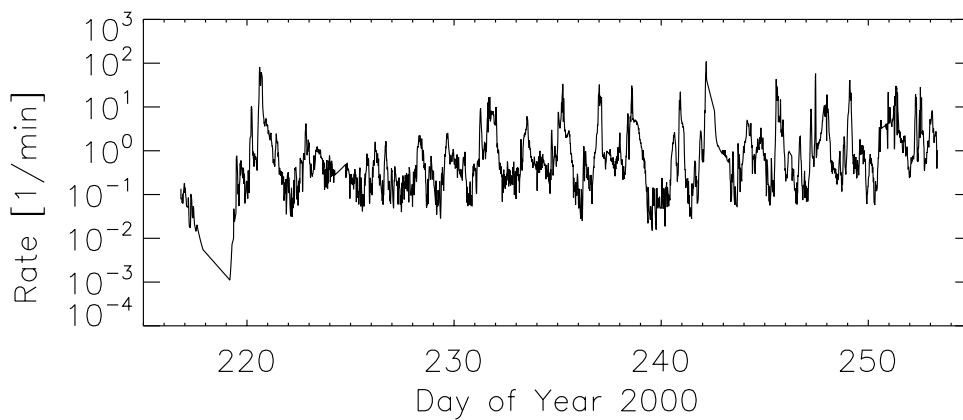


Figure 12: Impact rate of jovian dust stream particles (AC21 and AC31) measured during Galileo's G28 orbit at approximately $280R_J$ from Jupiter (no smoothing applied).

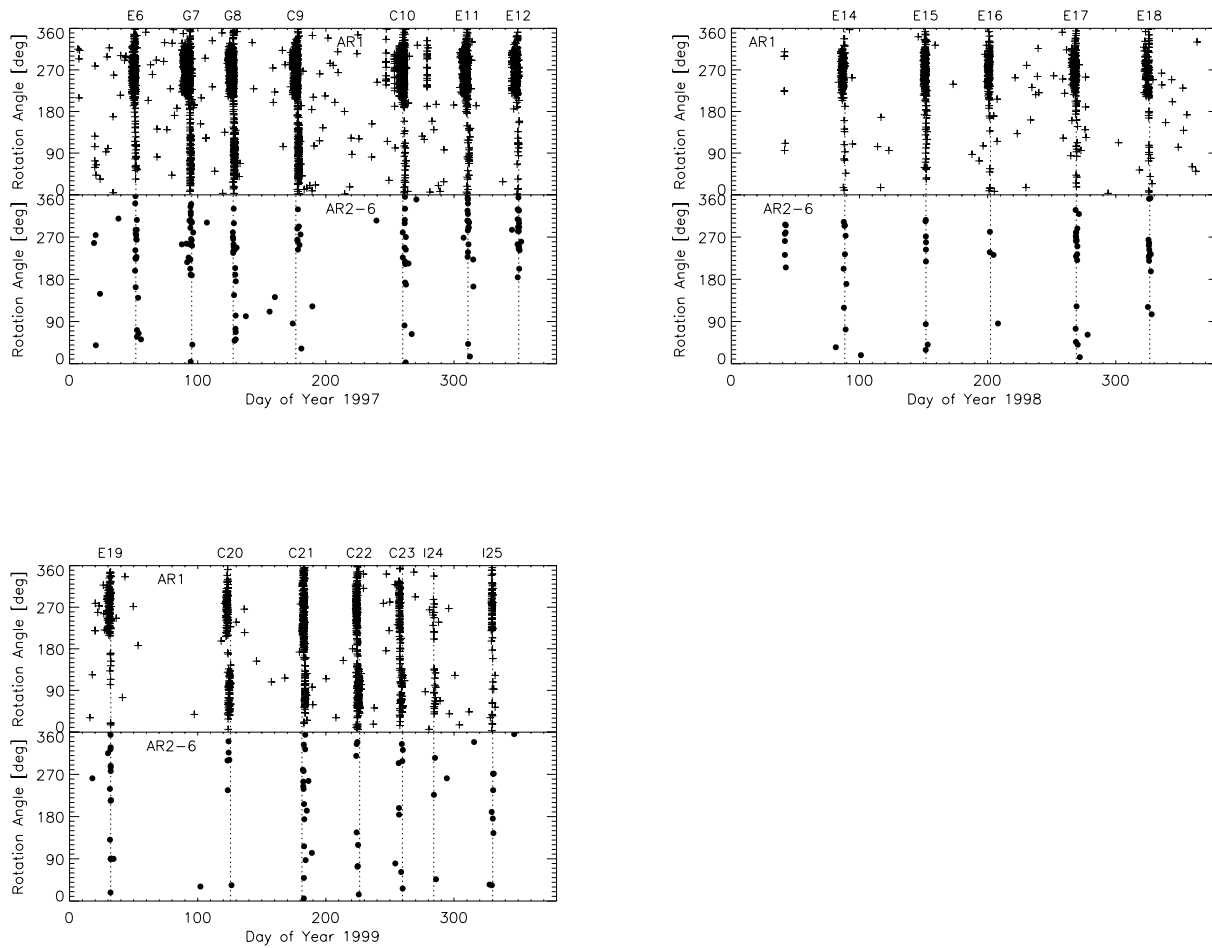


Figure 13: Correction for Paper VIII: rotation angle vs. time for two different mass ranges for the time interval 1997-1999. Upper panel: small particles, AR1 (Io dust stream particles); lower panel: big particles, AR2-4. Vertical dotted lines indicate Galileo's satellite encounters.